

Arctic, Antarctic, and Alpine Research

An Interdisciplinary Journal

ISSN: (Print) (Online) Journal homepage: www.tandfonline.com/journals/uaar20

Alpine vegetation community patterns in the Khumbu region, Nepalese Himalaya

Ruolin Leng, Stephan Harrison, Elizabeth A. Byers, Mahesh Magar, Harkrei Rai, Ram Raj Rijal & Karen Anderson

To cite this article: Ruolin Leng, Stephan Harrison, Elizabeth A. Byers, Mahesh Magar, Harkrei Rai, Ram Raj Rijal & Karen Anderson (2024) Alpine vegetation community patterns in the Khumbu region, Nepalese Himalaya, Arctic, Antarctic, and Alpine Research, 56:1, 2309686, DOI: [10.1080/15230430.2024.2309686](https://doi.org/10.1080/15230430.2024.2309686)

To link to this article: <https://doi.org/10.1080/15230430.2024.2309686>



© 2024 The Author(s). Published with license by Taylor & Francis Group, LLC.



[View supplementary material](#)



Published online: 20 Feb 2024.



[Submit your article to this journal](#)







[View related articles](#)



[View Crossmark data](#)



Alpine vegetation community patterns in the Khumbu region, Nepalese Himalaya

Ruolin Leng ^a, Stephan Harrison ^a, Elizabeth A. Byers ^b, Mahesh Magar^c, Harkrei Rai^c, Ram Raj Rijal^c, and Karen Anderson ^{a,d}

^aDepartment of Geography, University of Exeter, Penryn Campus, Cornwall, UK; ^bAppalachian Ecology, Elkins, West Virginia, USA; ^cThe Himalayan Research Center, The Himalayan Research Expeditions, Lainchaur, Kathmandu, Nepal; ^dEnvironment and Sustainability Institute, University of Exeter, Penryn Campus, Cornwall, UK

ABSTRACT

The Himalayan alpine zone (HAZ)—a high-altitude zone above approximately 4,100 m.a.s.l., is projected to experience strong eco-environmental changes with climate change. As plants expand their range in this region, other processes are likely to be impacted; for example, flows and stores of water. A first vital step in conceptualizing HAZ ecohydrology is to understand the distribution pattern of HAZ vegetation communities. Satellite remote sensing provides one means of doing so, but the often patchy distribution of alpine vegetation creates challenges when using coarse-grained satellite data whose pixels are typically coarser than the grain of vegetation pattern. Here we use fine spatial resolution satellite imagery from WorldView-2 (2 m² per pixel) coupled with elevation model data from the Copernicus GLO-30 product to produce a land cover classification for the HAZ. Field data captured during in situ surveys in the Gokyo valley, Nepal, were used to drive and then test a random forest classifier. Grassy meadows and dwarf shrubs belonging to the *Rhododendron* and *Juniperus* families dominate the ecology of the alpine zone in this region, so we created three vegetation classes for mapping indicative major plant communities dominated by these species. We found that altitude and aspect were dominant drivers of vegetation distribution in the HAZ and that the average vegetation cover of *Rhododendron* spp. and *Juniperus* spp. reduces with increasing altitude, as expected. South- and east-facing slopes were dominated by *Juniperus* spp., whereas north- and west-facing slopes were dominated by *Rhododendron* spp., and the growth extent of *Rhododendron* spp. (between 4,010 and 4,820 m.a.s.l.) and meadow (between 4,010 and 4,680 m.a.s.l.) were vertically wider than that of *Juniperus* spp. (between 4,010 and 4,660 m.a.s.l.). Results from this study demonstrate the vegetation distribution pattern in HAZ at the plant community level and provide an impetus for further studies that seek to understand ecohydrological interactions between dwarf plants and water flows and stores in the HAZ.

ARTICLE HISTORY

Received 25 April 2023
Revised 19 December 2023
Accepted 3 January 2024

KEYWORDS


Alpine vegetation;
Himalayan alpine zone; land
cover classification; remote
sensing; climate change

Introduction

Climate change is predicted to have significant impacts on high mountain systems. As the highest mountain system in the world, the Himalayas are projected to experience significant eco-environmental changes with continued climate change (Dolezal et al. 2016; Nie et al. 2021). The Intergovernmental Panel on Climate Change's sixth assessment report (Adler et al. 2022) argues that the Hindu Kush Himalaya will experience an increased temperature of about 1°C to 2°C, increased annual or summer monsoon precipitation, and increasing thaw and degradation of permafrost in the coming decades, with more pronounced changes under higher emissions scenarios. Shifts in climate have already impacted glaciers in the

region, with evidence for widespread, rapid ice mass loss (Bolch et al. 2012), alongside changes in vegetation distribution (Shrestha, Gautam, and Bawa 2012; Mishra and Mainali 2017; Anderson et al. 2020). Plants alter the flows and stores of water compared to bare ground (Fatichi, Pappas, and Ivanov 2016), and interactions between dwarf plants and snow exist in many high mountain systems (Julitta et al. 2014; Wheeler et al. 2016; Tomaszewska, Nguyen, and Henebry 2020). Leng, Harrison, and Anderson (2022) argued that ecohydrological interactions between plants and water are similarly likely to occur in the Himalayas. These ecohydrological processes will impact the hydrology of the wider region in ways that are so far unresolved (Körner 2021) and under

CONTACT Ruolin Leng  rl552@exeter.ac.uk  Department of Geography, University of Exeter, Penryn Campus, Cornwall TR10 9FE, UK.

 Supplemental data for this article can be accessed online at <https://doi.org/10.1080/15230430.2024.2309686>

© 2024 The Author(s). Published with license by Taylor & Francis Group, LLC.

This is an Open Access article distributed under the terms of the Creative Commons Attribution-NonCommercial License (<http://creativecommons.org/licenses/by-nc/4.0/>), which permits unrestricted non-commercial use, distribution, and reproduction in any medium, provided the original work is properly cited. The terms on which this article has been published allow the posting of the Accepted Manuscript in a repository by the author(s) or with their consent.

future scenarios of vegetation expansion may impact the water security for millions of people in catchments supplied by Himalayan rivers (Immerzeel et al. 2014). Furthermore, alterations in the diversity and functioning of alpine systems could impact habitats for various other ecological communities (e.g., wildlife; Aryal, Cockfield, and Maraseni 2016), also having implications for the carbon status of these systems (McLaren et al. 2017). Understanding the impacts of climate change on these processes could facilitate the development of effective strategies to mitigate resulting effects. As a result, scientific attention needs to be given to studying alpine ecology and hydrology between the tree line and snow line (4,100 to 6,000 m.a.s.l.)—which we name the Himalayan alpine zone (HAZ).

A first vital step in assessing HAZ ecohydrology is to understand the basic ecological situation of HAZ, which can be met by mapping the distribution patterns of HAZ vegetation communities. This is a complex task because alpine vegetation often assumes a dwarf form with low leaf area index and can be spatially patchy at scales finer than the resolution of many sensors onboard satellites (Reese et al. 2014). Though land cover (LC) maps exist for parts of the Himalayas from previous studies, these focus on aspects such as changes in agricultural land (Misra, Cawkwell, and Wingler 2020), horticulture (Rasool et al. 2021), glacial area (Kumar et al. 2021), land degradation (Rashid, Lone, and Romshoo 2011), and forest assessment (Batar, Watanabe, and Kumar 2017), with very few products describing HAZ plant series or community distribution above the tree line. The commonly used NASA Landsat data set (1972–present) provides image data at 30-m spatial resolution in five visible to near-infrared (NIR) spectral bands (Uddin et al. 2015), and other moderate-scale sensors such as Sentinel-2A at 10-m spatial resolution (Misra, Cawkwell, and Wingler 2020; Nandy, Srinet, and Padalia 2021) have been used for forest resource management (Uddin et al. 2015; Nandy, Srinet, and Padalia 2021) and land use monitoring (Misra, Cawkwell, and Wingler 2020) in the Himalayas but not in the HAZ. Commercial platforms like RapidEye at 5 m (Adam et al. 2014), PlanetScope at 3 m (Francini et al. 2020), QuickBird-2 at 2.4 m (Kavzoglu, Erdemir, and Tonbul 2017), and WorldView-2 (WV-2) at 2 m (Pu and Landry 2012) offer opportunities to monitor vegetation at finer spatial resolution but have not been included in many studies owing to the financial cost of buying such data. Nevertheless, in those studies that have tested the finer-resolution commercial satellite

imaging products, Pu and Landry (2012) reported significantly improved classifications of seven urban tree species with WV-2 data (resolution at 2 m) compared to IKONOS (resolution at 4 m) and attributed this improvement to the finer spatial resolution and spectral configuration of the instrument. Since then, more studies have shown the potential of WV-2 imagery for mapping vegetation to species level (Rapinel et al. 2014; Madonsela et al. 2017). Some studies demonstrated that the very high spatial resolution of WV-2 brought about higher classification accuracy of LC maps, compared with maps using Landsat or Sentinel series data sets (Suchá et al. 2016; Araya-López et al. 2018). However, most of the alpine studies using WV-2 focused on mapping tundra in the Arctic and Antarctic (Jawak et al. 2019; Terskaia, Dial, and Sullivan 2020; Verdonen et al. 2020). A few works used WV-2 for vegetation studies at fine scale in the Himalayas (Mishra et al. 2018; Nandy et al. 2019; Deval and Joshi 2022), but none were conducted in the alpine zone above the tree line.

Alpine vegetation communities exhibit high spatial heterogeneity and patchiness (Walker et al. 2006; Graae et al. 2022). This necessitates fine spatial resolution workflows for understanding vegetation distribution patterns. In similarly sparsely vegetated and heterogenous systems such as drylands (Walker, De Beurs, and Wynne 2014; Cunliffe, Brazier, and Anderson 2016), studies have shown that coarse-grained satellite data poorly describe ground conditions because of lower vegetation signal-to-noise ratios, interference from bright soil background reflectance, and relatively high spatial heterogeneity. All of these impede “robust calibration and evaluation of remotely-sensed” data products in these systems (Smith et al. 2019). The same challenges face remote sensing of plant communities in the HAZ (Saha et al. 2005; Singh and Pandey 2021), with the added complexity of major topographic-induced variations in sensor–surface relationships that could theoretically generate uncertainties in radiance, reflectance, and higher-level products (e.g., vegetation indices). Another challenge to map LC in the HAZ is the paucity of ecological information owing to its remoteness and difficult weather situations (Erinjery et al. 2018), which limits site-based understanding of conditions and processes and also prevents robust validation of remote sensing retrieved data (Leng, Harrison, and Anderson 2022; Zou et al. 2023). Hence, we conclude that the current main challenges of conducting land cover mapping in the HAZ are twofold: (1)

the limited accessibility of satellite products with very fine spatial resolution and (2) the scant in situ knowledge about the ecological situation and spectral properties of LC types in those areas. Furthermore, capturing detailed hyperspectral measurements of LC types in these areas is further hampered by the challenges of accessibility and power supplies at altitude. Methodologies employing high-specification instruments with high power demands are not feasible or appropriate within these regions because facilities do not exist to charge the instruments repeatedly.

In this study the goal was to generate an LC classification workflow using WV-2 data, informed by spectral measurements and in situ survey data, and to evaluate the potential applicability of this approach to exploring ecological patterns in HAZ. Our work was driven by five research questions.

- What is the spatial grain of patterns in plant communities in the HAZ from in situ observations?
- To what extent are dwarf plant communities in the HAZ spectrally separable based on spectral information from in situ and satellite data sets?

- Does WV-2 data provide the capacity for LC classification at the plant community level?
- How does the plant community composition in the HAZ vary with elevation, aspect, and slope?
- Using the derived LC map, can the spatial patterns of plant communities be discriminated?

Data and methodology

Study area

The study area is located in the Sagarmatha National Park (SNP) in the Khumbu Himal region of eastern Nepal (Figure 1a). For the purpose of this study, we focused on a study region within the national park with an areal coverage of 253 km² (Figure 1b). This region is centered on two major valley systems (Gokyo and Khumbu) that drain from the high peaks of Sagarmatha (Everest) and Cho Oyo, respectively.

The annual precipitation in Khumbu is around 525 mm (measurements from Pheriche station at 4,260 m.a.s.l.; Perry et al. 2020), 76 percent of which occurs during the monsoon season between June and September (Perry et al. 2020). Dwarf plants and alpine meadow are the dominant

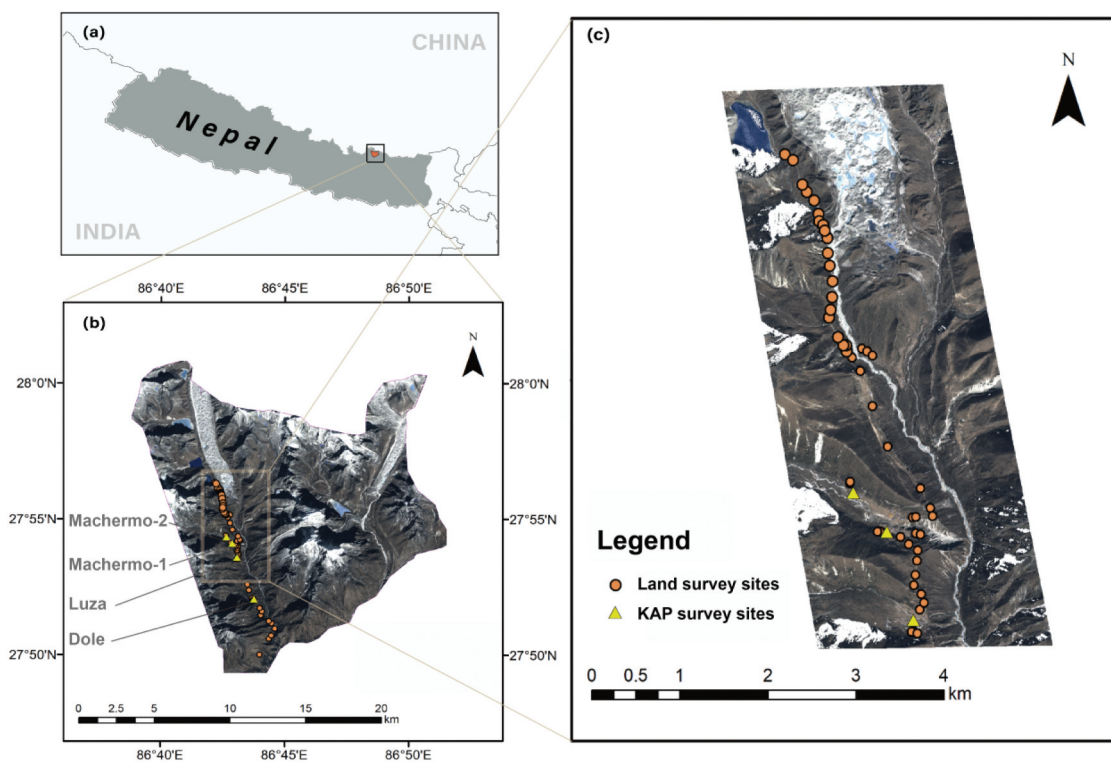


Figure 1. (a) The study area is located in Sagarmatha National Park, Khumbu Himal, Eastern Nepal. (b) The whole study area (SNP), with the orange points denoting seventy-five in situ land cover (LC) survey sites along the hiking trail from Namche Bazar up to the Gokyo valley (GKY) and the yellow triangles denoting the four kite aerial photography (KAP) survey sites. (c) A smaller example study area in GKY used for initial data evaluation and band selection in LC classification training.

vegetation communities in the alpine area (Byers 2022), comprising mixtures of species such as *Juniperus indica* and various dwarf *Rhododendron* shrub species (e.g., *Rhododendron setosum*, *Rhododendron anthopogon*), barberry species (e.g., *Berberis angulosa* and *Berberis tsarica*), *Primula denticulata*, *Ephedra gerardiana*, and *Cassiope fastigiata*. In all cases, plant heights rarely exceed 50 cm, and the flowering time of these dwarf plants ranges from April to August (Byers 2022; Leng, Harrison, and Anderson 2022). The climatological seasons in Nepal are defined by the monsoon period: the pre-monsoon season (March–May), summer monsoon season (June–September), post-monsoon season (October–November), and winter season (December–February; Nayava 1980). The pre- and post-monsoon seasons are an ideal time for alpine flora survey, where satellite sensors have the best chance of capturing cloud-free imagery.

A small area centered on the Gokyo valley, shown in Figure 1c, was used for initial data exploration. This region—which we refer to as “GKY”—covers 15.95 km² and extends from Luza village (27.893569° N, 86.718654° E) to Gokyo Lake (27.944359° N, 86.697768° E). The region extends from an elevation range of 4060 to 5147 m.a.s.l. GKY was used as a representative example because all of the typical LC classes in the HAZ were present and this was the region of a detailed field survey and contained more than half of our in situ survey sites in the region (forty-nine of seventy-five sites; Figure 1c). It therefore provided a useful smaller areal subset on which to test approaches before scaling up to the wider region.

Remote sensing and field spectroscopy data sets

Various remote sensing data were used, from satellite measurements to in situ spectra and aerial photography. The following sections describe these data sets in full.

WV-2 data

WV-2 satellite data were acquired in the post-monsoon season, on 11 December 2020 (at 52.5° solar zenith and 24.1° off-nadir angle), with cloud-free conditions. WV-2 is the first commercial eight multispectral band fine spatial resolution satellite sensor and has a swath width of 16.4 km, a revisit time between one and three days, and a spatial resolution of 2 m. It also has a panchromatic sensor (450–800 nm) with 0.5-m spatial resolution (Updike and Comp 2010). The WV-2 images were geometrically, radiometrically, and atmospherically corrected following the digital globe guidelines (Updike and Comp 2010; Núñez et al. 2021). Details of the full image processing pipeline are provided in Supplementary Data A.

Copernicus (GLO-30) imagery

We used the Copernicus digital elevation model (DEM)—part of the high-quality topographic data sets provided by Copernicus Programme, which is mainly obtained from the X-band, SAR-derived WorldDEM data set and locally infilled by other elevation data (Cuellar et al. 2022). This DEM offers near-global coverage and provides a regular grid of elevations that represent the surface of the Earth (Guth and Geoffroy 2021). The product at 30-m resolution (GLO-30) has been open access since 2021 (Guth and Geoffroy 2021).

In situ spectral reflectance measurements

In situ measurements of spectral reflectance of different LC classes were obtained to ascertain adequate spectral separability prior to classification model training (Serbin et al. 2014). The nature of this landscape and the difficulty of charging high-powered devices meant that we chose to carry very simple low-powered instruments that measured reflectance in a limited number of spectral bands that aligned well with the major regions sampled by optical satellite sensors. These instruments were the ALTA and Milton Multiband Radiometer (MMR), which are highly portable, sturdy, and reliable (Figures 2 and 3). In both cases, the spectral measurements were calibrated with reference to a Kodak gray card with 18 to 20 percent reflectance across the measurement range of the instruments. This calibration standard had previously been calibrated relative to a high-grade optical 99 percent reflecting Spectralon panel in controlled laboratory conditions. Each instrument is described in more detail in the following paragraphs.

ALTA instrument. ALTA is a rugged and simple active instrument designed by Lunar and Planetary Institute scientist Allan Treiman (Treiman 2000). Though this device is predominantly used in remote sensing and physical teaching, it can be used to easily and rapidly collect data on the proportions of colored light that reflect from real-world objects. It weighs 243 g (with battery) and so is highly field portable, relying on a 9 V battery for power. Reflectance can be measured in eleven colors of light with ALTA (Figure 2). This is an active spectrometer, producing light in eleven light emitting diodes within a window that contains a central detector. When placed in contact with the object being measured, each LED is illuminated by pressing a button, and the reflected flux can be recorded. The measurements of objects can be calibrated against standards and manipulated into graphs of reflectance versus light wavelength.

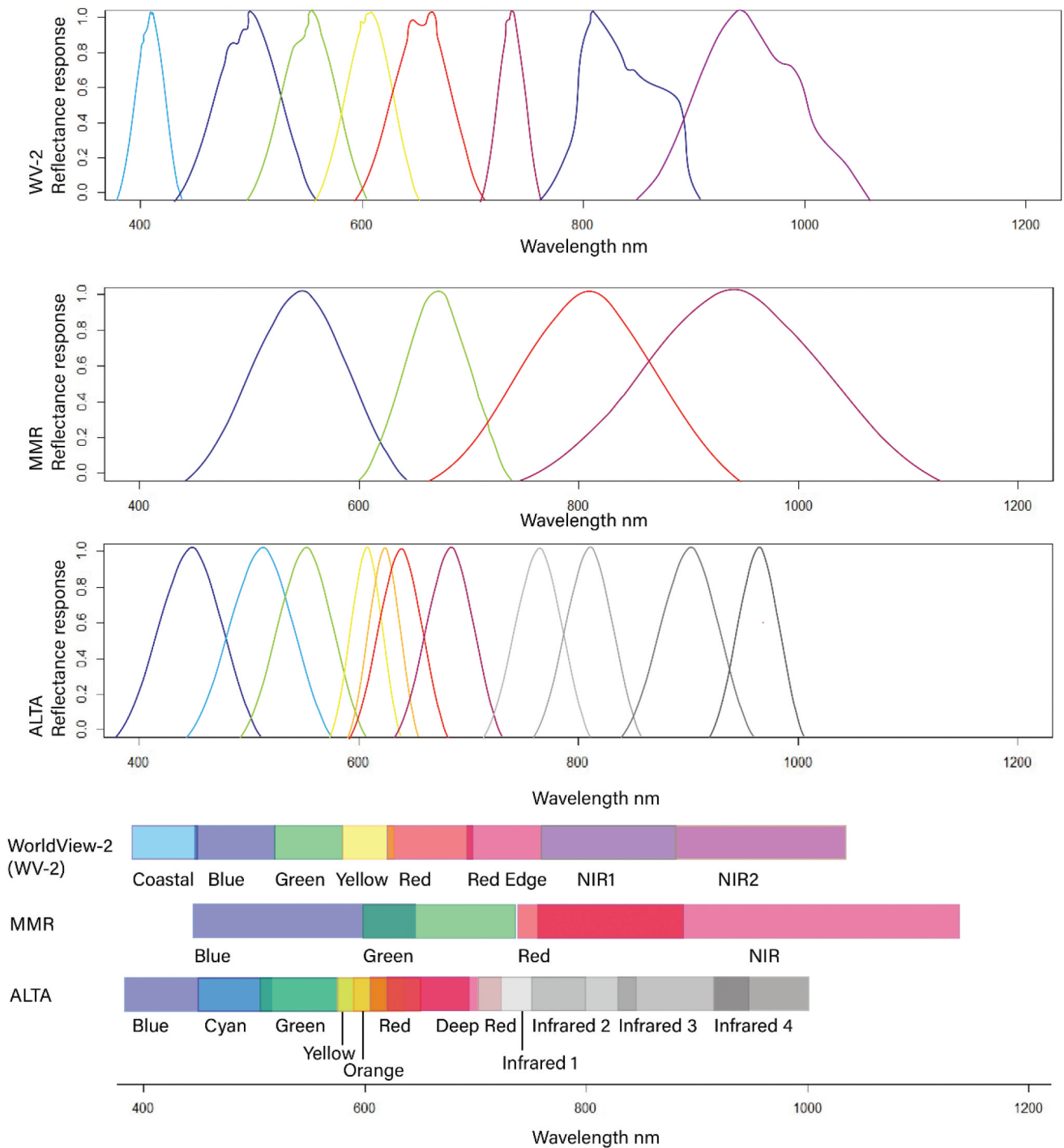


Figure 2. The spectral band information of in situ spectrometers used (MMR and ALTA) and comparison with WV-2.

Because the measurement window in the ALTA is around 2 cm diameter (Figures 3a, 3b), this instrument could not be used to measure plants with leaves smaller than that size. Different from the MMR, the ALTA can be used in any lighting condition because it generates its own radiation and so is independent of the problems of cloud cover and variable illumination experienced when capturing spectral measurements under solar illumination.

Milton multiband radiometer. The MMR was designed initially as a basic, robust, highly adaptable, low-cost and portable radiometer for ground data collection in remote sensing (Milton et al. 2009). Different from the ALTA, the MMR is a passive device that is held above the object being measured. The instrument measures the reflectance of a small area of around 1 to 2 m in diameter on the ground (varying according to the height it is held above the target). Measurements are calibrated relative

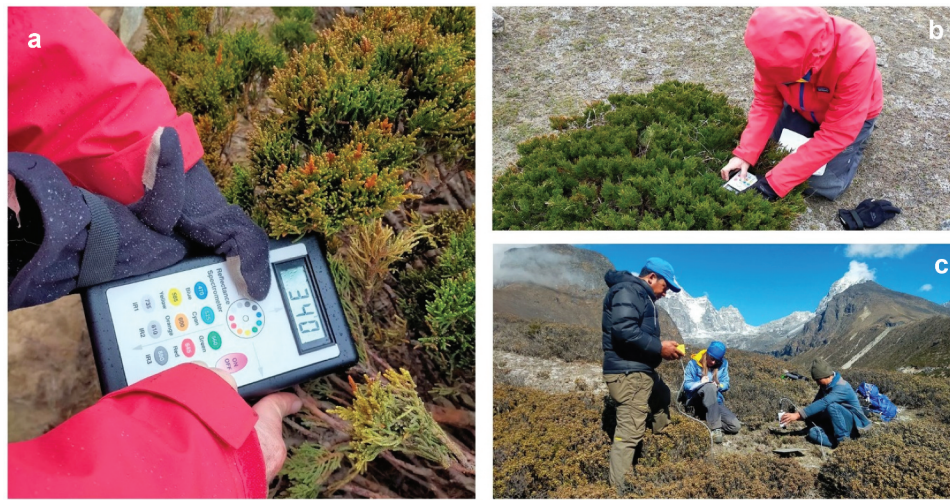


Figure 3. Spectroscopic measurements in action in the Gokyo valley. (a) and (b) Different views of the ALTA spectrometer being used to make contact measurements of the reflectance of *J. indica*. (c) The MMR being used to measure the Kodak gray card reference standard before the surrounding *R. setosum* was measured. Operation of the MMR requires more personnel.

to a standard reference card, in this case the aforementioned Kodak gray card (Milton et al. 2009; Figure 3c) and has four spectral bands (Figure 2). The MMR was suited to canopy measurements and was operated near to solar noon in sunlight. Though every effort was made to capture measurements under optimal clear blue sky conditions, it was not always possible to achieve consistency in these factors because of the changing mountain weather.

Kite aerial photography

It was not possible to use drones to perform aerial survey data collection because of prohibitively expensive permits and the lack of facilities for necessary battery charging in remote mountain huts. Instead, kite aerial photography (KAP) was used to collect aerial images of four survey areas—two at Machermo (4,426 m.a.s.l.), one at Luza (4,336 m.a.s.l.), and one at Dole (4063 m.a.s.l.; Figure 1). A 5.0 m² KAP foil was used in this study because it provided a relatively stable aerial platform. A 3D-printed picavet mount was used to carry a GoPro Hero 4 Silver within a protective shockproof case to ensure waterproof and dustproof operation (focal length 5.4 mm, horizontal opening angle 60°, aperture range f/2.5; Casella et al. 2020). A picavet is a system of cords and/or pulleys designed to keep a platform stable (Duffy et al. 2018). The Go Pro was set to take photos automatically at 3-second intervals, and a Go Pro remote control allowed for manual control of settings (e.g., shutter speed) and checking the remaining battery power (Koh and Wich 2012). Five ground control points were set in each survey site as reference for obtaining GPS information

for each photo (Duffy et al. 2018). Wind conditions dictated the altitude of the kite, and sufficient line was deployed until the platform was deemed stable to commence surveying: typically this was between 20 and 50 m of line (Duffy et al. 2018). Details about the kite and camera used in this study are provided in Supplementary Data Table S2.

Field ecological data

Land cover survey

Reference data for remote sensing-driven LC classification were generated from an in situ georeferenced field survey carried out in the Gokyo valley of Nepal (Figure 1c) between 26 April 2022 and 12 May 2022. These surveys were conducted along an elevation transect starting at 3,727 m.a.s.l. and extending to 4,462 m.a.s.l. Overall, data from seventy-five field locations (Figure 1b) were surveyed in locations proximal to the hiking trail between Phortse Thanga and Gokyo. At each location, lists of vegetation species were recorded. Polygons of spectrally homogeneous areas were digitized manually onto the WV-2 data set and labeled according to LC class IDs using the recorded field locations of reference data. A total of 264 polygons (comprising 13,089 pixels) from augmented visual interpretation formed the reference data set for training (75 percent of total, 9,520 pixels) and validation (25 percent of total, 3,569 pixels). Figure 4 shows typical vegetation communities in three survey sites located in Gokyo valley. At twenty-one sites along this same elevation transect from Dole to Machermo, the point-centered quarter method (PCQM; Cottam and Curtis 1956) was used to establish vegetation density and spatial

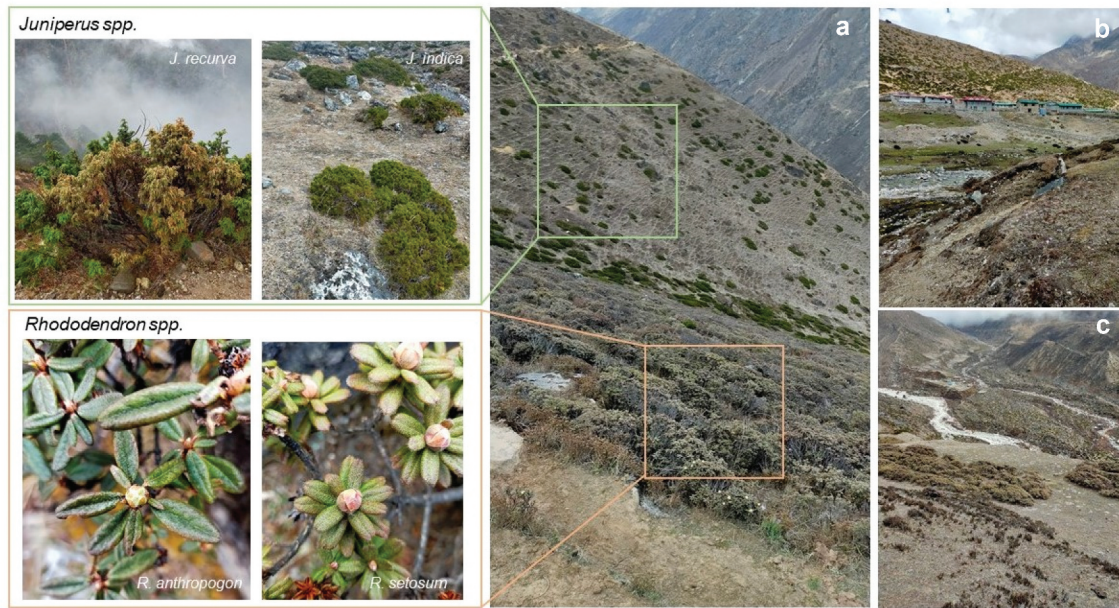


Figure 4. The dominant vegetation communities in the alpine zone in Gokyo valley. (a) Near Luza (4,302 m.a.s.l.), where meadow and *Rhododendron* spp. (*R. anthopogon* and *R. setosum*) are dominant (highlighted by orange square), and *Juniperus* spp. (*J. recurva* and *J. indica*) appear in small patches (highlighted by green square). (b) The landscape of Machermo village (4,414 m.a.s.l.), where the south-facing slope is dominantly covered by *J. indica* interspersed with grasses, and the valley below is covered by meadow and rock debris. (c) The scene on the north-facing slopes above the village of Machermo (4,452 m.a.s.l.), where meadow and dwarf *Rhododendron* species are the dominant land cover (LC), and *R. setosum* and *Cassiope fastigiata* are found in patches on the slopes leading down to the valley.

organization of species within the community. In PCQM, the distance of plants to random sample points is converted to plant density (details in Supplementary Data B).

For this, a line transect was established in each survey site along which, six to eight sampling points were chosen with random intervals between 0 and 10 m distance taken from a random number table. Each sampling point was divided into four quarters in which the distance to the center point, taxonomic identity, and plant height were recorded for the nearest woody plant species (Jafari, Zarre, and Alavipanah 2013). For plant species identification we used the *Wildflowers of Mount Everest* guide (Byers 2022).

On the basis of this survey, we defined three broad vegetation classes. Two were shrub classes and were dominated by either *Juniperus* spp. or dwarf *Rhododendron* spp. A third class was named “meadow,” and this was predominantly a grass/sedge community.

Signature separability analysis

Jeffries-Matusita (J-M) distance, a statistical parametric criterion to check interclass separability, was computed for all classes (Wacker and Landgrebe 1971; Sanam, Mathai, and Lakshmanan 2023). It is a normalization of the Bhattacharyya distance between the class means and the distribution of values from the means over

a range of zero to two, called pairwise separability, among the classes. A value of zero indicates similar classes, and a value close to two indicates highly separable classes. J-M distance has been widely used to examine the spectral similarities among the LC classes in remote sensing studies (Schmidt and Skidmore 2003; Wicaksono and Aryaguna 2020; Sanam, Mathai, and Lakshmanan 2023). Here, it was applied to the spectral reflectance of *Rhododendron* spp., *Juniperus* spp., meadow, and bare soil measured by MMR and ALTA or derived from WV-2. The J-M separability criterion (J) between two classes x and y is defined as follows (Richards 2013):

$$J_{xy} = 2(1 - e^{-d_{xy}}) \quad (1)$$

where d_{xy} is the Bhattacharyya distance between classes x and y and is calculated using the following formula (Richards 2013):

$$d_{xy} = \frac{1}{8} (m_y - m_x)^T \left[\frac{\Sigma_x + \Sigma_y}{2} \right]^{-1} (m_y - m_x) + \frac{1}{2} \ln \frac{\left| \frac{\Sigma_x + \Sigma_y}{2} \right|}{\sqrt{|\Sigma_x| |\Sigma_y|}} \quad (2)$$

where x is a vector of the first object’s spectral response, y is a vector of the second object’s spectral response,

Σ_x is the covariance matrix of sample x , and Σ_y is the covariance matrix of sample y .

Feature selection

We undertook feature selection in a sample area (GKY, 15.95 km²) containing 65 percent of our in situ survey sites. Because feature selection is computationally expensive, it was more efficient to use a subset of the original data in order to perform various iterations of this process. Eleven input single-band images (eight spectral bands derived from WV-2 and three topography-derived bands from GLO-30: elevation, slope, and aspect), along with 181 validation polygons (5,004 pixels in total) from in situ survey and Google Street View identification were input as training data. The implementation of recursive feature elimination (RFE) in this analysis was conducted using a 500-tree random forest algorithm, specifically, the “rfFuncs” method within the “caret” R package (RStudio Team 2015). The training model was repeated ten times to demonstrate the importance ranking of the bands and metrics performance based on the number of input features (details in Supplementary data C). The results of this analysis conducted in the GKY area informed the wider-area analysis.

Land cover classification using random forest approaches

Using the optimal band set highlighted by feature selection described in the previous section as input bands (details in Supplementary data Table S5), *dzetsaka* in QGIS 3.20.3 (a fast and easy plugin version 3.7 with integrated random forest (RF) classifier; Karasiak 2017) was used to generate two LC maps in GKY and SNP separately. The semi-automatic classification plugin in QGIS 3.20.3 (2022) was used with an independent validation data set in GKY (1,668 pixels) and SNP (3,569 pixels) to generate confusion matrices to test the quality of the classification outcome and determine the proportion of correctly classified pixels (Ji and Niu 2014; Shahi, Shafri, and Hamedianfar 2017). User accuracy (UA), producer accuracy (PA), overall accuracy (OA), and kappa (κ) are the parameters for accuracy assessment of the classification models and were calculated from the confusion matrices (Ji and Niu 2014; Shahi, Shafri, and Hamedianfar 2017). UA is calculated by dividing the total number of classified points that agree with the reference data by the total number of classified points for that class, PA is calculated by dividing the total number of classified points that

agree with reference data by the total number of reference points for that class, and OA and κ provide an overall assessment of the accuracy of the classification (Shahi, Shafri, and Hamedianfar 2017).

Statistical spatial analysis using the land cover map of SNP

To evaluate the impacts of topographical drivers on plant community distribution, spatial analysis was undertaken based on the LC map produced for the larger SNP extent. Firstly, 5,000 random points were generated within SNP polygon in QGIS. With each point as center point, 5,000 buffering areas with a side length of 30 m were created for spatial analysis. Because the spatial resolution of the LC map was the same as the WV-2 data set (2 m), there were 225 pixels in each square sample. Vegetation cover (VC) of three plant communities (*Rhododendron* spp. [VC_R], *Juniperus* spp. [VC_J], and meadow [VC_M]) in each square sample were calculated by dividing the number of total pixels (225) by the number of vegetated pixels. The topographical features (elevation, aspect, and slope) of each square sample were extracted from the GLO-30 data set. Hence, an array of 5,000 samples with six properties (VC_R , VC_J , VC_M , elevation, aspect, and slope) was generated. All of the vegetated pixels were grouped by aspect: east (45°–135°), south (135°–225°), west (225°–315°), and north (0°–45°, and 315°–360°). Analysis of the vegetation distribution with topography variation was undertaken using this data set. Figure 5 presents an overview of the key methodological steps in this study.

Geostatistical analysis

To obtain a quantitative description of the ecological distribution pattern in this study area, geostatistical analyses of sample variograms were undertaken based on the LC map within SNP extent. This enabled assessment of plant continuous canopy coverage variation over three sampling sites—Dole, Luza, and Machermo. Square polygons of 200 m × 200 m were defined in *Rhododendron* spp.– and *Juniperus* spp.–dominant areas in each site, and the raster layers with LC classes of each polygon were extracted.

Then, to extract measures from the plant continuous canopy coverage variograms, models were fitted to the raster layers using the “Gstat” geostatistical package in R studio 2023.03.1 (Pebesma 2015; R Studio Team 2015). For each of the raster layers, a spherical variogram model was built to describe data (Anderson and Kuhn 2008). The range of variogram, which is defined as the limit of spatial correlation, where the pair of values that are this distance or greater apart no longer causes a corresponding change, was calculated by these models

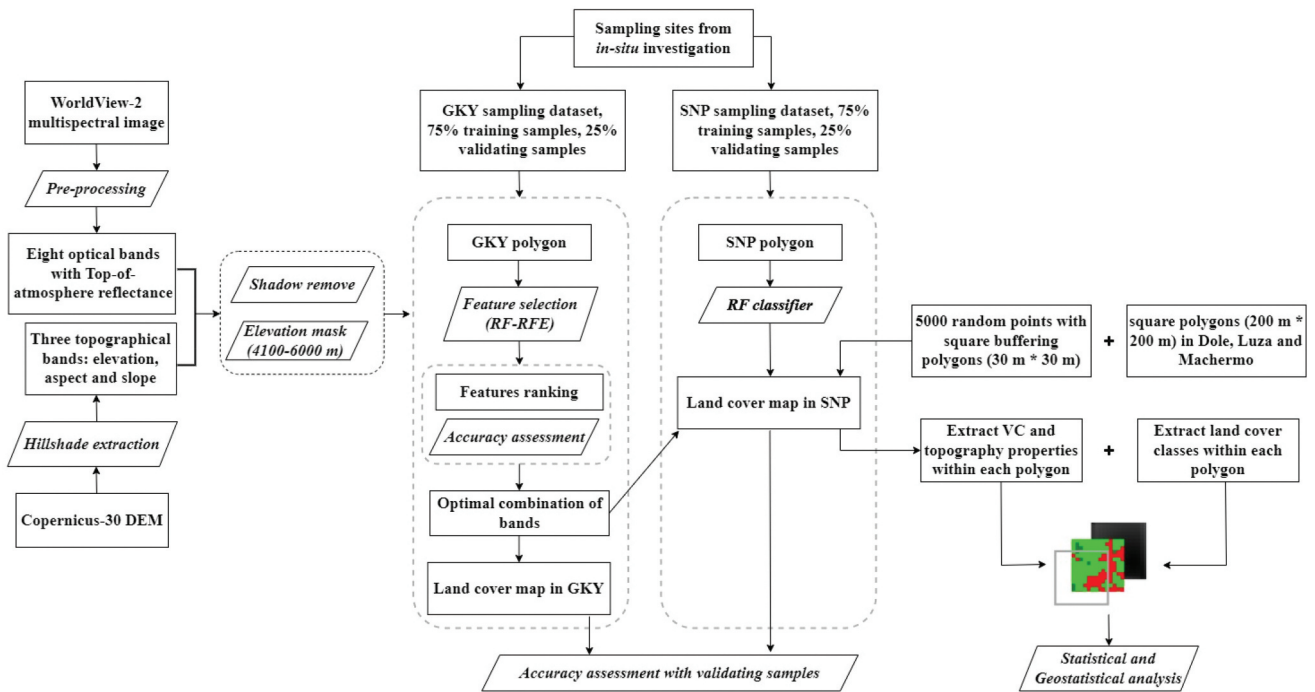


Figure 5. Workflow outline.

(Anderson and Kuhn 2008; Oliver and Webster 2014). Here, range represents the continuous canopy coverage distance within the sampling area. The spherical model is described by Equation (3), where γ is the semivariance for a vector of discrete lags (h), a is the variogram range, c_T is the total sill variance, c_0 is the nugget variance (spatially uncorrelated variance), and c_1 is the spatially correlated variance for $h \leq a$. Equation (4) defines c_T where $\gamma(h)$ is the c_T if $h > a$ (Deutsch and Journel 1992; Anderson and Kuhn 2008).

$$\gamma(h) = c_1 * \left[1.5 \frac{h}{a} - 0.5 \left(\frac{h}{a} \right)^3 \right] + c_0 \quad (3)$$

$$c_T = c_0 + c_1. \quad (4)$$

Results

The vegetation land cover distribution in the HAZ

The vegetation LC distribution across twenty-one survey sites from Dole to Machermo was determined by PCQM survey (details in Supplementary Data Table S3). The length of the survey plots ranged between 12.9 and 45.8 m, with vegetation species number varying from one to five. Our observations indicate that *Rhododendron* spp. and *Juniperus* spp. were the dominant vegetation classes throughout the altitude range of 4,063 to 4,445 m. a.s.l. The density of various plant communities in twenty-

one survey sites calculated from the PCQM measurements, the density of two dominant genera—*Juniperus* spp. (D_J) and *Rhododendron* spp. (D_R)—and the difference between them ($D_R - D_J$) is shown in Table S3 (Supplementary Data). In eighteen of twenty-one survey sites, *Juniperus* spp. were distributed more sparsely than *Rhododendron* spp. The density of *Juniperus* spp. varied between 0 and 1.92 individuals/m², and in *Rhododendron* spp. the density varied from 0 to 37.38 individuals/m². The highest density of *Rhododendron* spp. (37.38 individuals/m²) was observed in Machermo-1, located on the north-facing slope with an altitude of 4,426 m.a.s.l.; the highest density of *Juniperus* spp. (1.92 individuals/m²) was observed in Machermo-3, located on a south-facing slope with an altitude of 4,070 m.a.s.l. Generally, the density discrepancy varied with slope facing aspect, which ranged from 24.30 to 37.38 individuals/m² in the sites located on north-facing slopes, higher than those for sites located on east-facing (from 3.81 to 29.02 individuals/m²) and south-facing slopes (0.13 to 0.66 individuals/m²). *Juniperus* spp. were more densely packed than *Rhododendron* spp. in only three out of twenty-one survey sites—Machermo-4, Luza-5, and Luza-6, which were all located on south- and east-facing slopes.

Typically, our fieldwork showed that *Juniperus* shrubs had a median height of 27.4 cm (range = 22.2–38.8 cm) and *Rhododendron* shrubs had a median height of 37.4 cm (range = 29.4–46.4 cm). Most of these plants are relatively small in terms of their footprint, with the dwarf

Rhododendron spp. having canopy crowns of less than 50 cm in diameter (in many cases, the typical size was around 20–30 cm diameter per plant crown). For *J. indica*, the plants exhibited much more diverse allometries depending on where they were growing; some plants were 2 to 3 m in diameter, whereas others were much smaller, around 50 to 80 cm typically. In terms of landscape perspective, *Juniperus* plants were typically more widely spaced in the landscape, whereas *Rhododendron* plants showed greater coalescence across the canopy, so that the crowns of neighboring plants often met, sometimes, but not always, forming a more continuous canopy cover. Figure 6 shows the situation at Machermo and Dole: a much more closed canopy can be observed in many places where *Rhododendron* was present (Figure 6b) and a more open canopy with sparsely distributed *Juniperus* plants where *Juniperus* was the dominant species (Figure 6a). Anecdotally and from field notes, we observed a shift in dominance between these two shrub communities with aspect.

The spectral characteristics of dominant dwarf plants in the HAZ

Figure 7 shows the spectral reflectance curves of LC classes derived from in situ measurements using MMR and ALTA, alongside the spectral information derived from WV-2. Details of spectral separability analysis within the LC classes (J-M distance) are given in Table S8 in the supplementary data.

Measurements using MMR demonstrated that bare soil presented distinct spectral separability with the vegetated areas (J-M between 1.84 and 1.99), which had higher reflectance in all bands of MMR compared with other classes.

Juniperus spp., *Rhododendron* spp., and meadow were spectrally similar to each other in blue (470 nm), green (560 nm), and red (660 nm) bands, but *Rhododendron* spp. and meadow displayed lower reflectance than *Juniperus* spp. in NIR (880 nm). *R. anthopogon* with *R. setosum* and *J. recurva* with *J. indica* are two pairs of plants with similar spectral characteristics, with J-M of 0.84 and 0.97, respectively. Spectral measurements using ALTA showed that *Juniperus* spp. and meadow were spectrally similar to each other across visible bands (470–660 nm) but showed some divergence in the bands between 700 and 810 nm (J-M = 1.85), *Juniperus* spp. displayed lower reflectance across the infrared red-1 and infrared red-2 bands than meadow. Analysis using spectral information derived from WV-2 showed that *Juniperus* spp. and *Rhododendron* spp. were spectrally distinct from meadow and bare soil (J-M = 1.99). Meadow and bare soil had similar spectral curves across all WV-2 bands (J-M = 1.96), and the average reflectance was higher than in the dwarf shrub communities. *Juniperus* spp. and *Rhododendron* spp. were spectrally similar with each other across 400–690 nm (J-M = 1.99), but *Juniperus* spp. displayed higher reflectance than *Rhododendron* spp. across red edge, NIR1, and NIR2 (705–1,040 nm).

According to the in situ LC survey and spectral measurement analysis, and making reference to the vegetation community distribution in the alpine Himalaya summarized by An et al. (2015), we chose six LC classes for classification in this study: *Rhododendron* spp., *Juniperus* spp., bare soil, water, meadow, and other (rock, snow, and ice); shadow has been removed from the WV-2 image before classification (Supplementary Data C). Data captured from the two major dwarf shrub communities were grouped owing to their

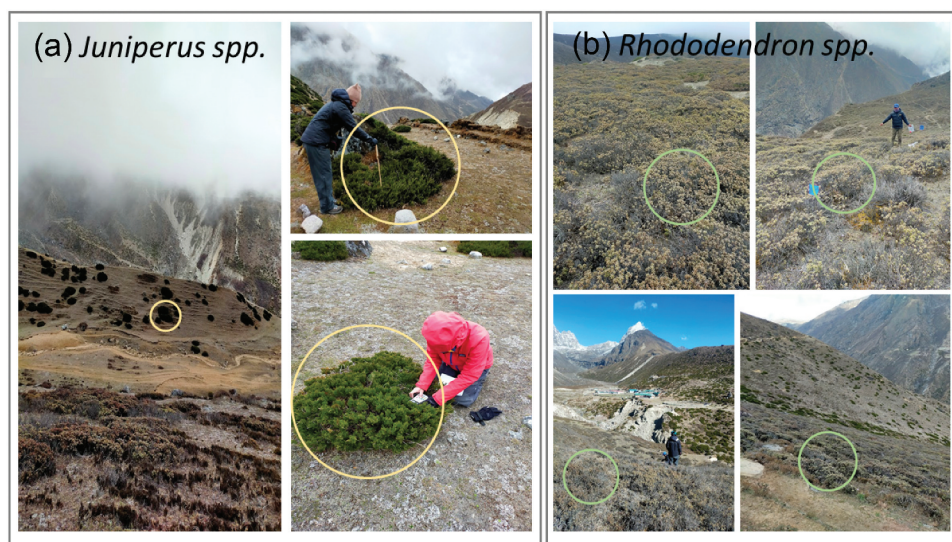


Figure 6. The typical distribution pattern of *Juniperus* spp. and *Rhododendron* spp. in the HAZ. The (a) *Juniperus* and (b) *Rhododendron* plants are highlighted.

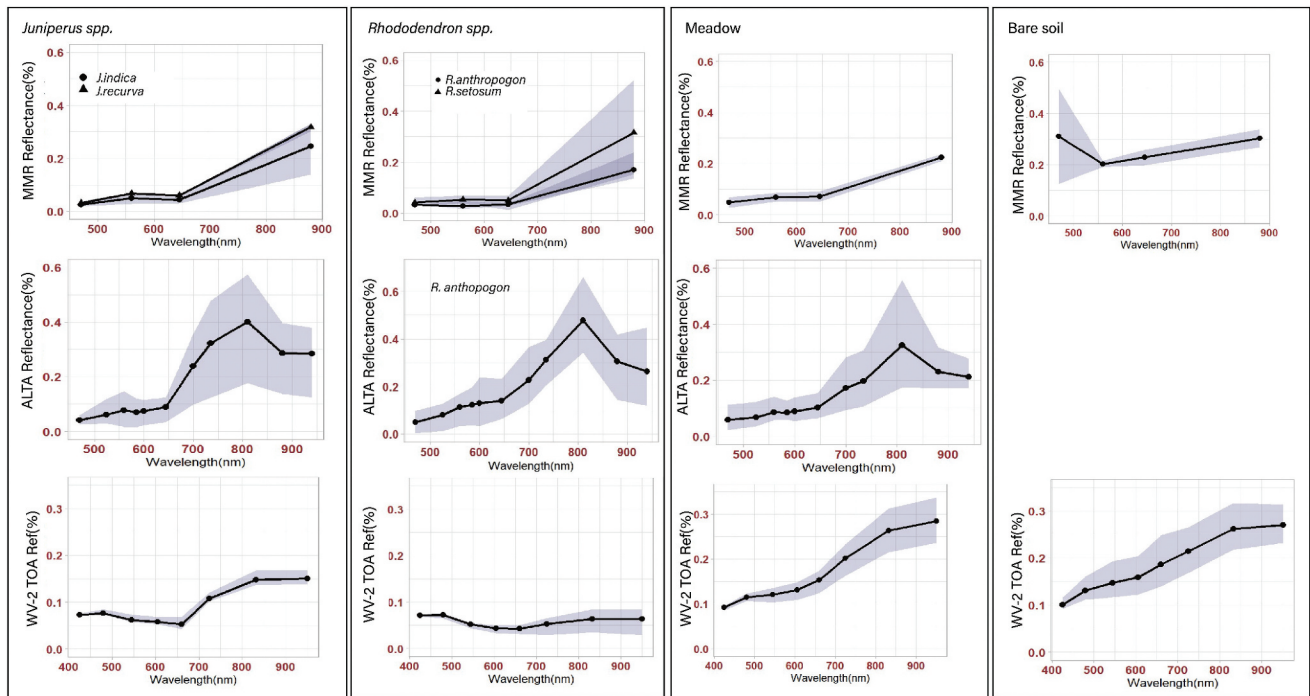


Figure 7. (a) and (b) Mean (\pm standard deviation) of land cover (LC) classes spectral reflectance (400–1,040 nm). In situ measurements of reflectance were made using MMR and ALTA. (c) Top-of-atmosphere (TOA) reflectance extracted from WV-2 imagery. Spectra were grouped into three vegetation cover classes (*Juniperus* spp., *Rhododendron* spp., and meadow) and bare soil. Among the in situ measurements using MMR, *J. indica* and *J. recurva* were grouped as *Juniperus* spp., and *R. anthopogon* and *R. setosum* were combined in *Rhododendron* spp.

similar spectral characteristics: *Juniperus* spp. (including *Juniperus recurva* and *J. indica*) and *Rhododendron* spp. (including *R. anthopogon* and *R. setosum*). The notation “*Rhododendron* spp.” and “*Juniperus* spp.” denotes that these were the dominant species in the plant community, not that the classes were restricted only to describing these species in isolation of others that co-occur. Therefore, readers should consider these as LC labels that encompass the vegetation community dominated by said species. The description of each LC class is presented in Table 1.

Feature selection result

As seen in Figure 8, there was considerable variation in the feature importance score among the eleven input features for LC classification. Elevation was considered

as prior descriptor for LC distribution in HAZ with the highest importance score. Among the eight optical spectral bands derived from WV-2, B8 (NIR2), B1 (coastal blue), B2 (blue), B3 (green), and B5 (red) followed elevation in the importance ranking. NIR2, green, and red bands were considered correlated with vegetation existence, corresponding with prior spectral knowledge about plants (Thomson et al. 2021). Coastal blue and blue bands discriminated between water bodies, glaciers, and snow (following expectations; Mitkari et al. 2022). B7 (NIR1) and B6 (red edge) were less useful than other spectral bands in feature selection ranking, probably due to similarity with red and NIR2, respectively, and so we excluded these from the RF-RFE classification model to reduce redundancy. The location of slope in the importance ranking

Table 1. Description of land cover (LC) classes used in this study.

ID	Class	Description
1	<i>Rhododendron</i> spp.	A mixed community dominated by dwarf <i>Rhododendron</i> spp. with a typical canopy height <50 cm. The three dominant species were <i>R. anthopogon</i> , <i>R. setosum</i> , and <i>R. lepidotum</i> , normally with dark green leaves with length <4 cm.
2	<i>Juniperus</i> spp.	A mixed community dominated by bushy woody shrubs of the genus <i>Juniperus</i> , growing to 50–200 cm tall with height depending on elevation/temperature, with largely horizontal branching. The leaves are dark gray-green with awl-shaped leaves in whorls or scale-like leaves pressed close to the branches in four overlapping ranks. Dominant species included <i>J. indica</i> with minor components of <i>J. recurva</i> ; <i>R. lepidotum</i> was sometimes observed occurring with <i>J. indica</i> on drier slopes throughout the study area.
3	Bare soil	Bare soil occurring as patches of exposed soil and includes dusty trails and pathways used by herders and grazing animals.
4	Water	Surface water including rivers, streams, and lakes.
5	Meadow	Graminoid (grass, sedge, rush) and forb patches with canopy height <20 cm, generally perennial, often with stoloniferous or rhizomatous growth forms and sometimes sparse in cover.
6	Other	Including rock debris, permanent snow, and glaciers.
7	Shadow	Shadows generated by topography variation falling on adjacent surfaces, which results in very dark or low brightness values.

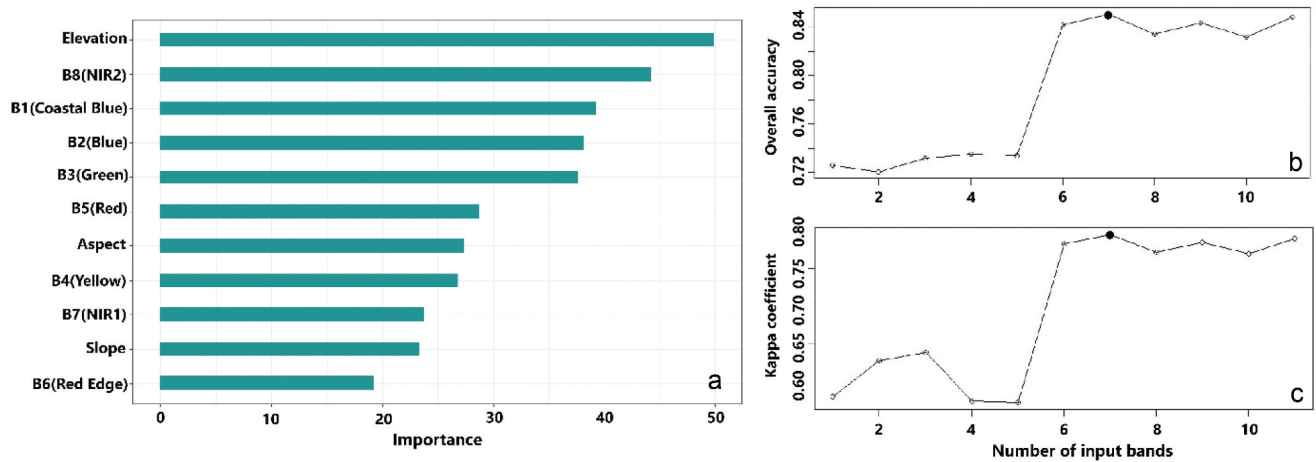


Figure 8. (a) Summary of feature importance scores of eleven input bands. The band ranking was generated by the RF-RFE model. Figures on the right display the variations in test accuracy based on the feature importance ranking and RF classification model. (b) and (c) The x-axis presents the number of input bands and the y-axis indicates the overall accuracy (OA) and κ (range = 0–1).

(number ten of eleven) indicates its lower importance for vegetation distribution in the HAZ than other features.

As displayed in Figures 8b and 8c, the OA and κ improved with the increase in input features. There was a significant increase from five input bands (OA = 73.40 percent, κ = 0.58) to six input bands (OA = 84.17 percent, κ = 0.78). The highest OA and κ were reached with seven input bands (OA = 85.03 percent, κ = 0.79), after which further increases in feature variables did not improve OA significantly.

Land cover classification in GKY region

The LC classification map in GKY is shown in Figure 9, with the accuracy assessment in Table 2. Using the optimal band set as the input data set, this map depicted that six LC types were classified with an OA of 85.03 percent, κ of 0.79. Reflecting the analysis results from the confusion matrix, water and *Juniperus* spp. were classified with relatively higher UA (98.98 and 98.14 percent, respectively), followed by bare soil (96.88 percent) and *Rhododendron* spp. (92.69 percent). Meadow was classified with a comparatively higher PA (99.67 percent), followed by water (84.78 percent), *Juniperus* spp. (81.87 percent), bare soil (80.52 percent), and *Rhododendron* spp. (79.92 percent). Among the six LC classes, “others” was classified with the highest PA (100 percent) and the lowest UA (75.63 percent); Table 2 indicates that some pixels belonging to the class “others” were misclassified as *Rhododendron* spp. and water.

For further evaluation of the classification accuracy quality, the zoomed-in WV-2 image, LC map in GKY and the in situ survey photos were contrasted in

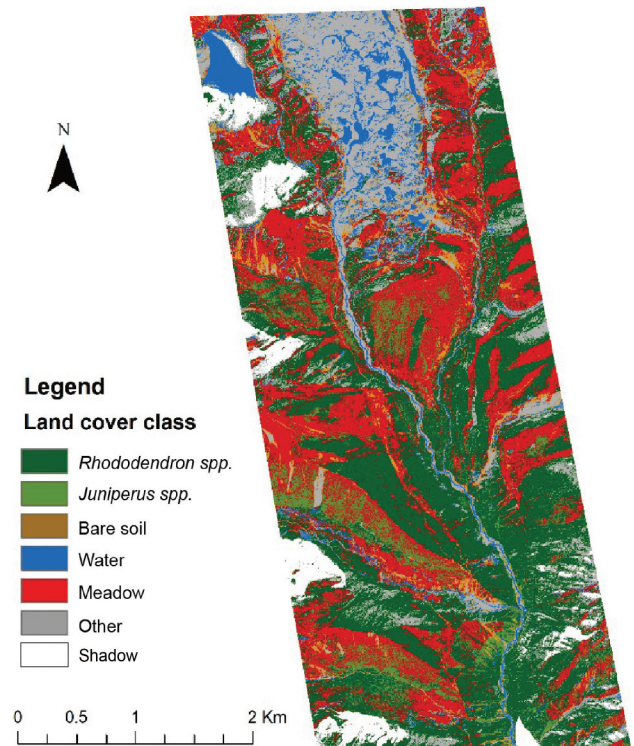


Figure 9. The land cover (LC) map in GKY.

Figure 10. The WV-2 image was displayed in false color synthesis (NIR1–red–green), for a distinct illustration of vegetated area as red color. Three in situ sites with typical alpine landscape in GKY were depicted (Machermo-1, Machermo-2, and Luza), and in each figure the areas at the same locations were highlighted with a number to show the comparison between classification result and in situ LC. Similar vegetation distribution patterns were observed in all three sites; that is, there were rivers

Table 2. Accuracy assessment of classification map in GKY with the optimal band set.

Classification pixels for each class	Validation pixels for each class						Total	User accuracy (UA) (%)
	<i>Rhododendron</i> spp.	<i>Juniperus</i> spp.	Bare soil	Water	Meadow	Others		
<i>Rhododendron</i> spp.	406	13	0	19	0	0	438	92.69
<i>Juniperus</i> spp.	3	158	0	0	0	0	161	98.14
Bare soil	0	1	62	0	1	0	64	96.88
Water	0	0	2	195	0	0	197	98.98
Meadow	0	21	12	0	299	0	332	90.06
Others	99	0	1	16	0	360	476	75.63
Total	508	193	77	230	300	360	1,668	
Producer accuracy (PA) (%)	79.92	81.87	80.52	84.78	99.67	100		
Overall accuracy (OA): 85.03%	Kappa: 0.79							

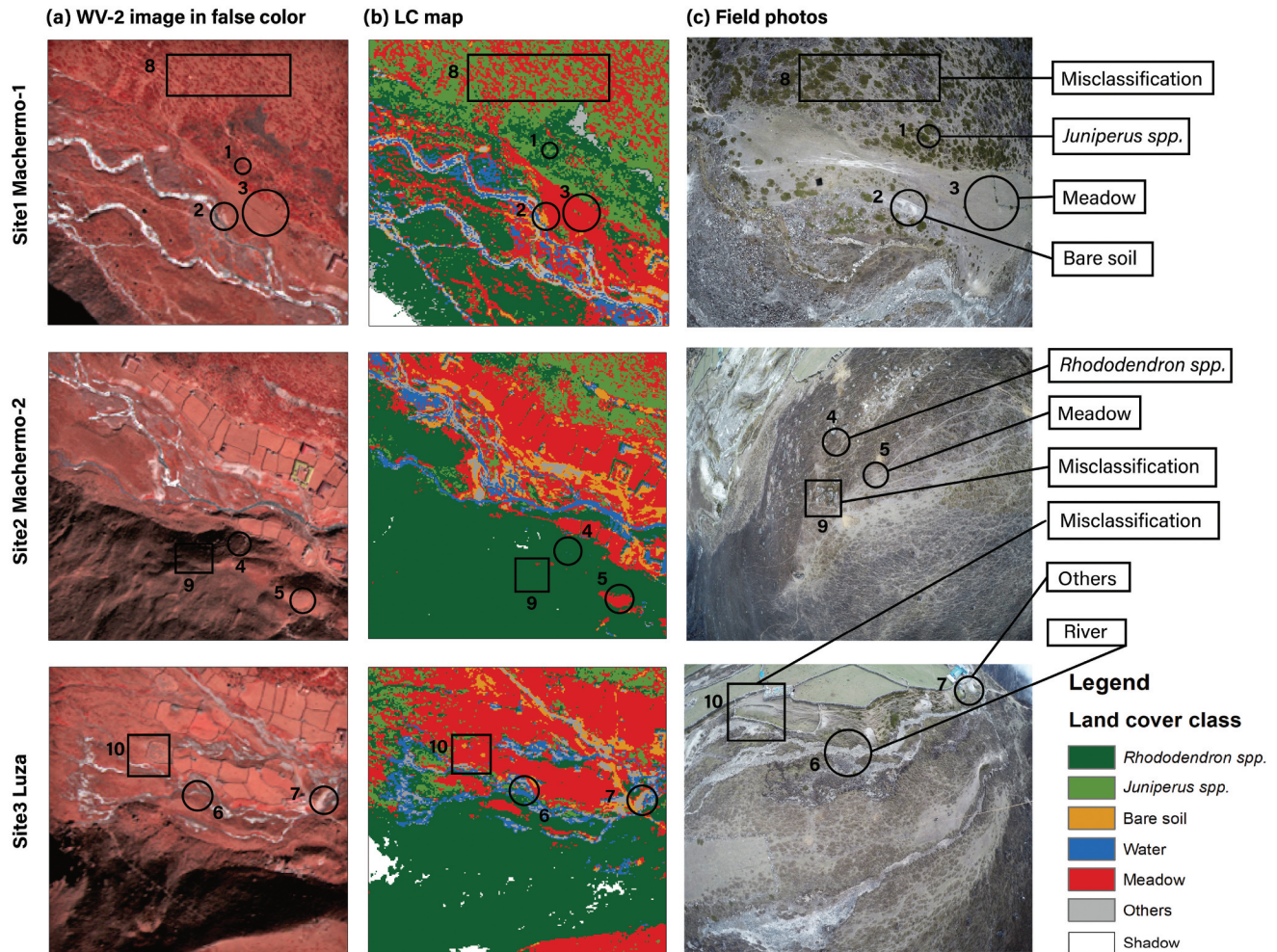


Figure 10. Zoomed-in contrast graphs of WV-2 image, land cover (LC) map, and in situ photos, showing three example sites with typical alpine land covers. (a) Machermo-1 is dominated by *Juniperus* spp., *Rhododendron* spp., and meadow. (b) Machermo-2 is dominated by *Rhododendron* spp. and meadow. (c) Luza is dominated by *Rhododendron* spp. and meadow; *Juniperus* spp. are sparsely distributed along the edge of agricultural pasture.

running through the valley, with rock debris around the rivers; the north-facing slopes below river were dominated by *Rhododendron* spp., with the south-facing slopes above the river dominated by *Juniperus* spp.; and meadow regions could be observed by the rivers in Machermo-2 and Luza, corresponding thematically with our own field surveys and photographs.

In Figure 10, ten sites were identified and highlighted on the WV-2 image, LC map, and in situ photos from KAP. These sites were assigned a unique number, which allowed for a direct comparison of the LC classification result with reference photos from in situ survey. Sites 1 to 7 were found to exhibit typical LC types where the thematic patterns corresponded closely with KAP products

captured in situ. However, misclassification was observed in sites 8 to 10: site 8 displayed a misclassification between *Juniperus* spp. and meadow. Similarly, site 9 showed a misclassification between *Rhododendron* spp. and rock debris, and site 10 demonstrated confusion between meadow and bare soil. Furthermore, the difference in distribution pattern among plant communities is displayed in Figure 10c: *Juniperus*-dominated areas had more open canopy, where gaps between plants existed; these patterns were not mirrored in the *Rhododendron*-dominated areas where canopies were more coalesced.

To evaluate the representativeness of GKY as an example study area for SNP, a density histogram of topographic factors—elevation, aspect, and slope—is shown in Figure 11. This demonstrates the similarity in the three topographical factors in GKY and SNP—a continuous range of skewness. In both GKY and SNP, the elevation displays a similar unimodal distribution, with a peak value around 5,000 (Figure 11a), and the aspect has a bimodal distribution, with peak values around 100° and 220° (Figure 11b); although the peak values are not exactly the same, the similar distribution shape of slope in GKY and SNP shows that GKY is a topographically representative example region for the wider SNP.

Land cover map of SNP

The final LC map in SNP is displayed in Figure 12. The three main vegetation cover classes—*Juniperus* spp.,

Rhododendron spp., and meadow—are depicted in green, dark green, and red, respectively. Almost half of the alpine area in SNP was covered by water and other (rock, ice, and snow). There was a significant shift between the three dwarf plant cover classes as altitude increased. A web map of SNP LC can be accessed at <https://leng.users.earthengine.app/view/snplandcovermap>.

Using the optimal band set as the input data set and an RF classification algorithm, the accuracy assessment showed that six LC types were classified with an OA of 92.56 percent and κ of 0.90 (Table 3). In the confusion matrix, *Juniperus* spp. were classified with the highest UA (98.79 percent), followed by *Rhododendron* spp. (96.20 percent), meadow (95.52 percent), and others (94.48 percent). Meadow was classified with the highest PA (99.13 percent), followed by *Rhododendron* spp. (98.83 percent), *Juniperus* spp. (90.26 percent), and others (90.19 percent). Across the six classes, the greatest source of uncertainties came from bare soil and water: 17.09 percent of bare soil and 18.18 percent of water was misclassified as others.

Spatial distribution pattern of dwarf plants in SNP

Figure 13 displays the vertical variation of dwarf plant cover classes (*Rhododendron* spp., *Juniperus* spp., and meadow) within the north, east, south, and west aspect groups.

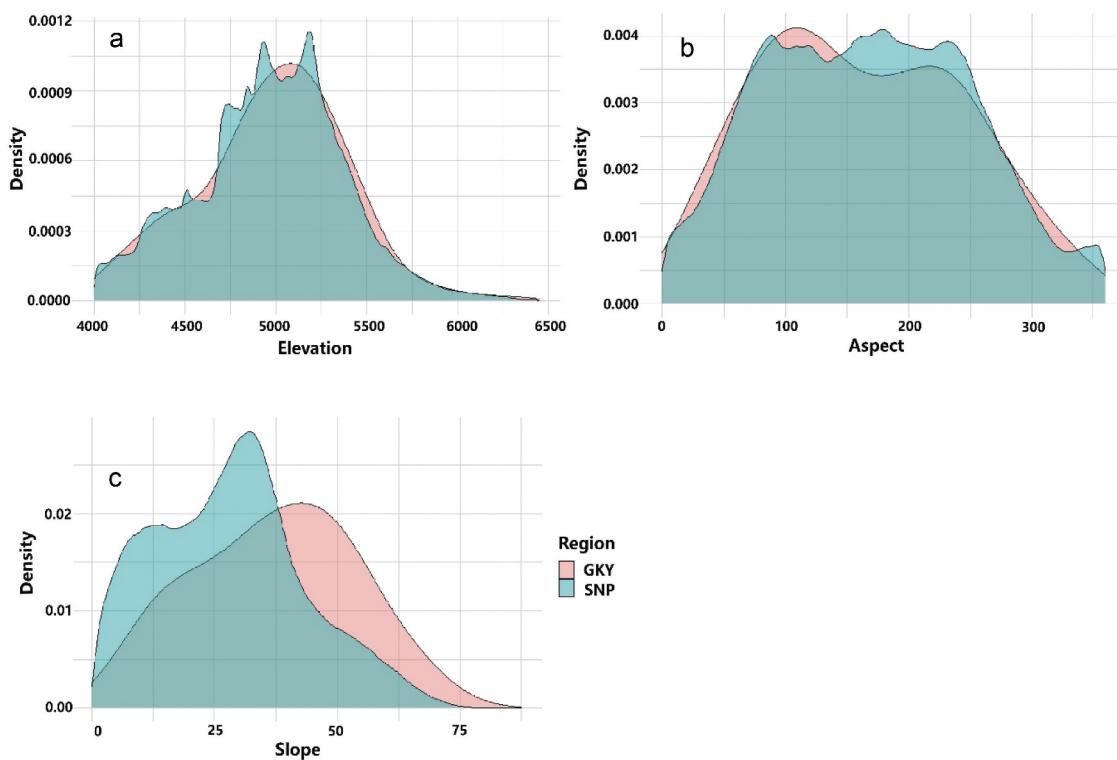


Figure 11. The density distribution histograms of elevation, aspect, and slope in GKY (pink) and SNP (blue).

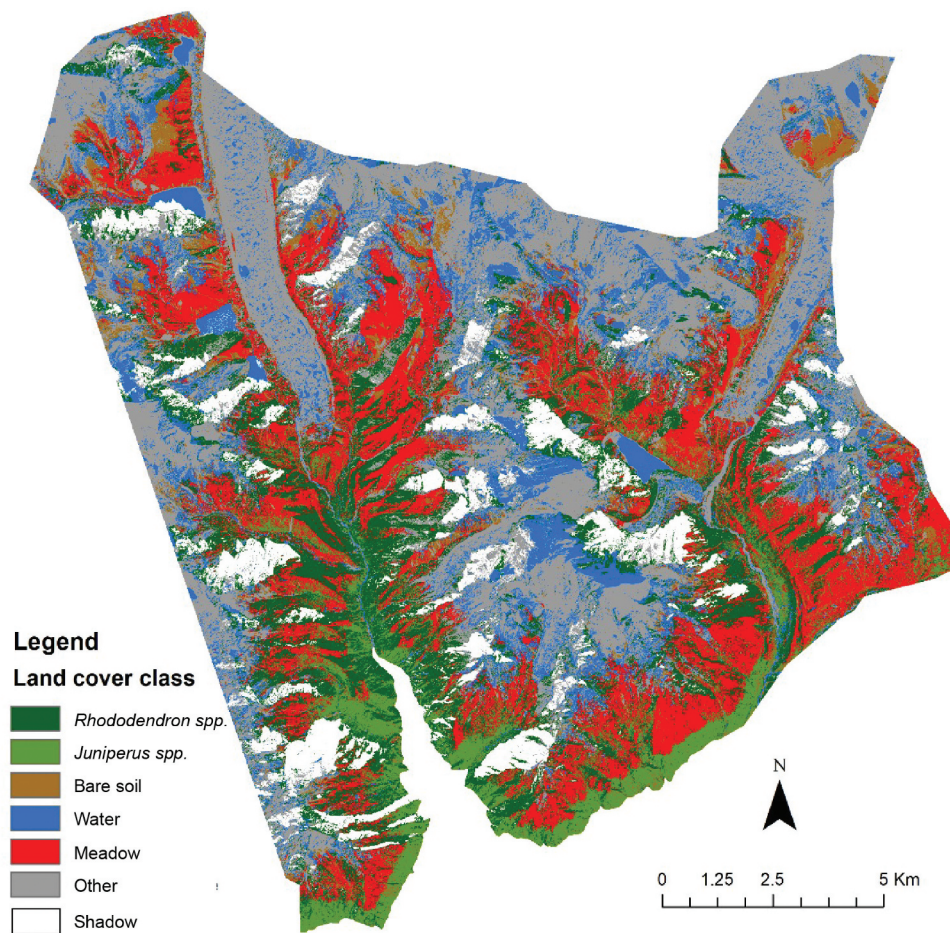


Figure 12. The land cover (LC) map in Sagarmatha National Park (SNP).

Table 3. Accuracy assessment results using error matrix of classification map with the optimal band set in Sagarmatha National Park (SNP).

Classification pixels for each class	Validation pixels for each class						Total	User accuracy (UA) (%)
	<i>Rhododendron</i> spp.	<i>Juniperus</i> spp.	Bare soil	Water	Meadow	Others		
<i>Rhododendron</i> spp.	963	13	0	25	0	0	1,001	96.20
<i>Juniperus</i> spp.	2	408	3	0	0	0	413	98.79
Bare soil	0	1	188	0	5	40	234	80.34
Water	0	0	1	485	0	108	594	81.65
Meadow	0	19	12	0	661	0	692	95.52
Others	3	0	13	19	0	600	635	94.48
Total	968	441	217	529	666	748	3,569	
Producer accuracy (PA) (%)	98.83	90.26	83.64	87.85	99.13	90.19		
Overall accuracy (OA): 92.56%								Kappa: 0.90

The average VC of *Rhododendron* spp. generally decreased with increasing altitude, and the VC of *Rhododendron* spp. located on north-facing slopes was higher than that of plants growing on other aspects (with the highest peak VC of 93.96 percent around 4,400 m.a.s.l.). The average VC of *Juniperus* spp. on all aspects had a similar trendline—lower density with increasing altitude until 5,000 m.a.s.l. and then tending toward zero after 5,000 m.a.s.l. *Juniperus* spp. was observed with higher VC in east- and south-facing areas (peak VC of 91.08 and 80.94 percent at 4,000 m.a.s.l.

respectively) than north- and west-facing areas. The average VC of meadow had a similar distribution shape, increasing with altitude from 4,000 to 4,900 m.a.s.l. and then decreasing from 4,900 to 5,000 m.a.s.l. There was almost no meadow recorded between 5,500 and 6,000 m.a.s.l. Meadow was found predominantly on south- and east-facing slopes (peak VC of 55.28 and 49.99 percent, respectively) compared with west- and north-facing slopes (peak VC of 36.24 and 18.39 percent, respectively). **Figure 12d** demonstrates the trends of hypsometric curves and the temperature versus elevation in the SNP area, where there

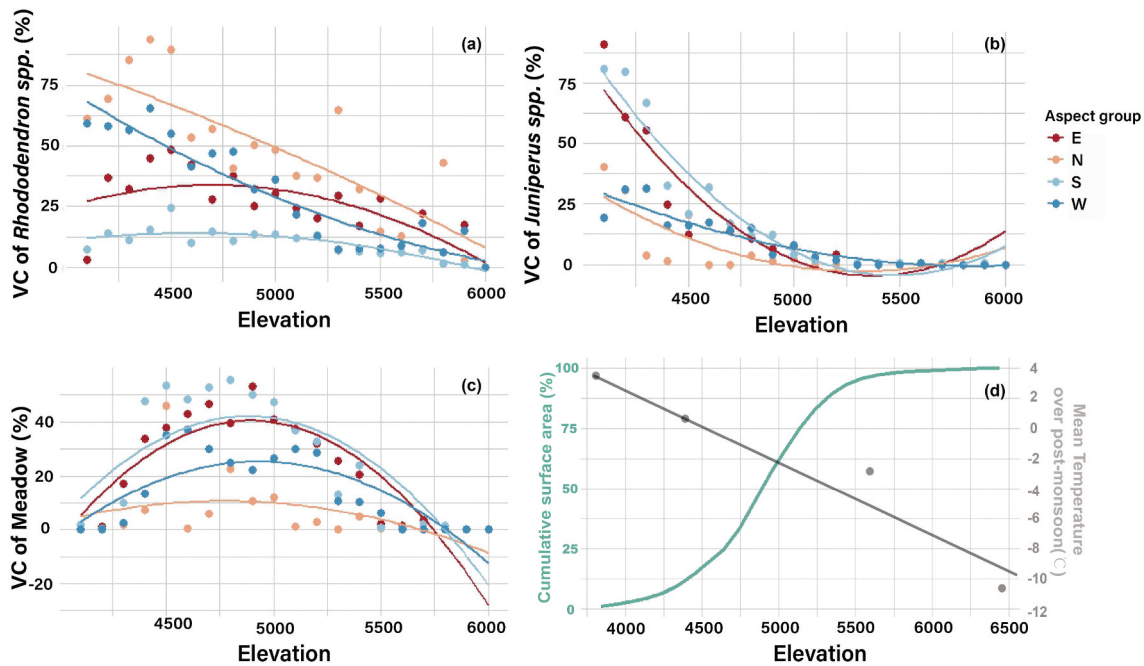


Figure 13. (a), (b) and (c) The scatterplots of three plant communities' (*Rhododendron* spp., *Juniperus* spp., and meadow respectively) vegetation cover (VC) derived from land cover (LC) map in SNP versus the elevation increase. Each point in the scatterplot represents the average VC within the corresponding elevation. Linear regression models are depicted in four colors to display the VC variation trend with an increase altitude for four aspect groups (east, north, south, west). (d) The hypsometric curve describing the landscape distribution (green line) with altitude and the changing temperature relationship with altitude (gray line) derived from four automatic weather stations in Khumbu—Phortse (3,810 m.a.s.l.), Pheriche (4,260 m.a.s.l.), Pyrimad (5,035 m.a.s.l.), and Camp II (6,464 m.a.s.l.)—during the post-monsoon season in 2019 (Perry et al. 2020).

was less land surface at higher elevations and the air temperature decreased (from 3.7°C to −10.5°C) with increasing altitude (from 3,810 to 6,464 m.a.s.l.) in the post-monsoon season.

Table 4 presents the distribution ranges with altitude and slope among three plant communities (minimum, maximum, median, quartile-1 [Q1], and quartile-3 [Q3]). The minimum and median altitude for *Rhododendron* spp. and meadow distribution were similar (both around 4,010 to 4,870 m.a.s.l.), which indicated that 50 percent of the total *Rhododendron* spp. or meadow pixels extracted from the LC map were growing within these altitude ranges in SNP, and 50 percent of *Juniperus* spp. were growing within the altitude range from 4,010 to 4,600 m.a.s.l. The altitude range between Q1 and Q3 for *Rhododendron* spp. growth was 4,010 to

4,820 m.a.s.l., which indicated that 75 percent of *Rhododendron* spp. were located within this area. The Q3 of altitude range for *Juniperus* spp. and meadow growth was lower than the ranges for *Rhododendron* spp. (4,660, 4,680, and 4,820 m.a.s.l., respectively). The median slope gradient for *Rhododendron* spp. growth (28°) was higher than those for *Juniperus* spp. and meadow (27° and 26°, respectively), which indicated that *Rhododendron* spp. is more adjusted for growing on steeper slopes than the other two plant species.

Quantitative analysis of the ecological pattern within plant communities

Visual assessment variograms per vegetation class in Figure 14 showed differences in texture between the

Table 4. Altitude and slope distribution range within three vegetation communities.

	Altitude range of plant distribution (m.a.s.l.)			Slope range of plant distribution (°)		
	<i>Rhododendron</i> spp.	<i>Juniperus</i> spp.	Meadow	<i>Rhododendron</i> spp.	<i>Juniperus</i> spp.	Meadow
Median	4,870	4,600	4,870	28	27	26
Minimum	4,010	4,010	4,010	0	0	0
Maximum	6,340	5,840	5,720	70	68	75
Interquartile	540	440	450	19	17	18
Quartile-1 (Q1)	4,280	4,230	4,240	10	9	9
Quartile-3 (Q3)	4,820	4,660	4,680	29	26	27

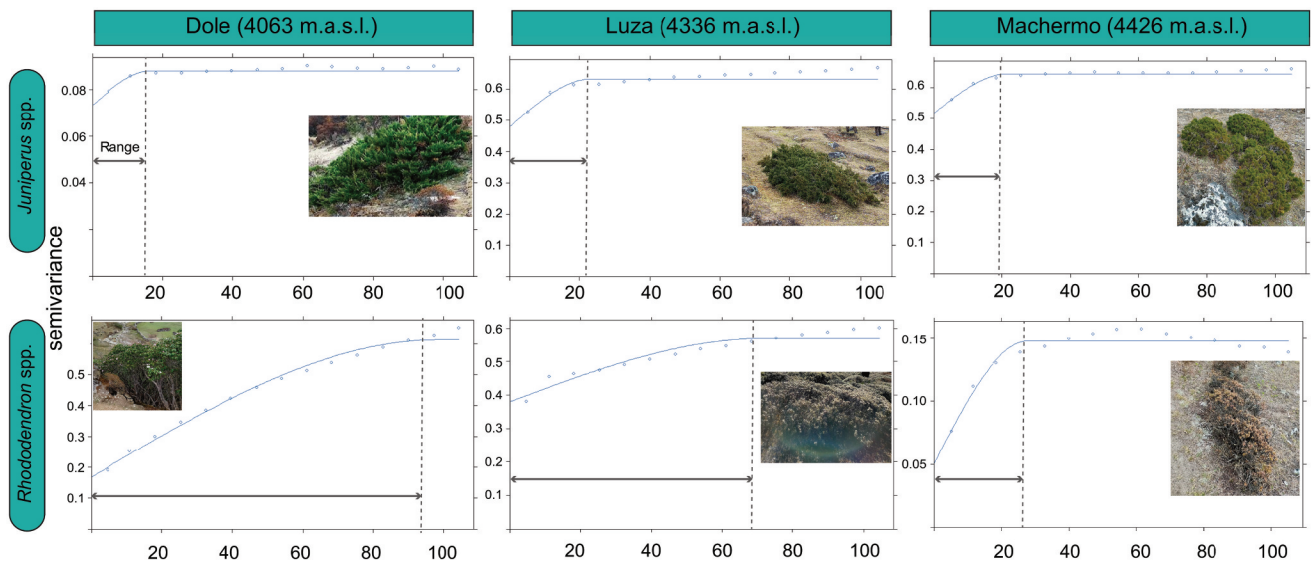


Figure 14. Continuous coverage variograms within *Rhododendron* spp.– and *Juniperus* spp.–dominant areas in (a), (d) Dole, (b), (e) Luza, and (c), (f) Machermo. In each figure, the curve represents the spherical function fitted to the semivariance model, the distance range is marked, and the photos from our in situ survey present the ecological situation in each site.

Table 5. Range variances extracted from model variograms within *Rhododendron* spp. (R) and *Juniperus* spp. (J) in Dole, Luza, and Machermo.

Site	Dole (4,063 m.a.s.l.)		Luza (4,336 m.a.s.l.)		Machermo (4,426 m.a.s.l.)	
	R	J	R	J	R	J
Range (m)	98.37	22.14	71.96	23.52	27.87	21.41

Rhododendron-dominated and *Juniperus*-dominated plant communities. Table 5 summarizes the variogram parameters for each model (within 0–100 m). In general, the area in which *Rhododendron* spp. were dominant (range = 28–98 m) displayed textures with a greater length scale compared to *Juniperus*-dominated zones (range = 21–24 m) in Dole, Luza, and Machermo. Greater range distances for *Rhododendron* spp. were found at lower altitude (28 m in Machermo, 72 m in Luza, and 98 m in Dole), indicating that *Rhododendron* forms larger clumps at lower altitude and is more sparsely distributed at higher elevations. *Juniperus* spp. showed similar patterns (range = 24 m or less, typically) across all three sites.

Discussion

What is the spatial grain of patterns in plant communities in the HAZ from in situ observations?

In this study, we investigated the dwarf plant distribution pattern from in situ photogrammetry and PCQM measurements. The PCQM result showed that the number of plant species varied from one to five within the 12.9 to 45.8 m range (Table S5). We have not been

able to find other studies that deliver comparable data on woody plant density in similar Himalayan systems, beyond one that reported a shrub diversity survey in the HAZ (altitude of 3,560–4,485 m), which found a higher average number of thirty-two shrub species within a 20 × 20 m plot (Rana, Samant, and Rawat 2011). Our shrub diversity result indicated that mapping LC classes in the HAZ at the plant community level required remote sensing data at fine spatial resolution (e.g., 2 m of WV-2 compared with 10–60 m of Sentinel-2; details are provided in Supplementary data D) for the distinction of *Juniperus* spp. and *Rhododendron* spp. This is likely due to the specific spatial grain of plant canopy structure in these dominant species.

Secondly, the measurements from PCQM displayed a denser distribution of *Rhododendron* spp. than *Juniperus* spp. in 86 percent of the survey sites in this study ($n = 75$). A similar vegetation distribution pattern was also shown in the photos from the KAP survey—the plant density in *Juniperus*-dominated areas was visually sparser than that in *Rhododendron*-dominated areas, and the gaps between *Juniperus* spp. were not mirrored in the *Rhododendron*-dominated areas (Figure 10). Also, according to the PCQM result, *Juniperus*-dominated south-facing

areas had lower density than *Rhododendron*-dominated north-facing areas. Higher vegetation density in north-facing forests compared to south-facing areas has been reported in Manang Valley—a semi-arid area located in central Nepal (Ghimire et al. 2010; Måren et al. 2015), because the higher solar radiation, higher evapotranspiration, and less available snowmelt water dry out the south-facing forests faster, hence reducing tree growth (Måren et al. 2015). Indeed, the rounded patches of *J. indica* shown in Figure 10 with gaps between them reflect the gradual expansion of this recently protected species into suitable habitat, after many years of burning and harvesting. In less disturbed alpine areas, dwarf *J. indica* forms a continuous cover, mixed with other dwarf shrubs.

The ecological pattern difference between *Rhododendron* spp. and *Juniperus* spp. communities was also demonstrated through geostatistical analyses (section “Quantitative analysis of the ecological pattern within plant communities” in this article), and patterns shown here reflected observations made in the field, which was that *Rhododendron* spp. formed a more continuous canopy cover than *Juniperus* spp. across all three sites (Table 5). The geostatistical results did reveal an altitudinal trend in *Rhododendron* spp. where the range reduced at higher altitude (Table 5), and this corresponds with our in situ survey photos shown in Figure 14 where *Rhododendron* spp. formed a coalesced canopy over visually larger areas in Dole compared to Luza and Machermo. Dole village lies close to the tree line. These geostatistical results also correspond with PCQM data that showed that *Juniperus* spp. (1.92 individuals/m²) was more sparsely distributed than *Rhododendron* spp. (37.38 individuals/m²).

The differences between ecological patterns of *Rhododendron* spp. and *Juniperus* spp. could be attributed to the aspect of their dominant areas. Plant species richness was found to be higher in south-facing compared to north-facing areas in subarctic Canada, attributed to the higher soil temperature and active layer depth in south-facing areas (Dearborn and Danby 2017). The decreases in vegetation cover were linked with decreasing temperature with increasing altitude in our study area (Figure 13); this temperature-driven vegetation distribution pattern mirrors previous reports from the alpine Himalaya (Telwala et al. 2013; Hamid et al. 2020). However, Kutiel and Lavee (1999) highlighted that moisture plays a deterministic role in the composition, structure, and density of plant communities in areas with less than 600 mm annual precipitation. Although there is a dearth of data on alpine communities in this regard and so it is difficult to make comparisons or corroborations, we posit that a similar moisture-driven pattern is possible in the HAZ area of Khumbu because the region experiences an annual precipitation of 525 mm (Perry et al. 2020).

Previous studies have demonstrated the important effects on hillslope–stream connectivity from the variation in vegetation pattern, density, and landscape heterogeneity in semi-arid ecosystems (Emanuel et al. 2014; Saco et al. 2020), because plants impact soil–water balance, available energy (from solar radiance), and precipitation distribution patterns (Keim, Skaugset, and Weiler 2006). The hydrological changes brought by vegetation density variation are also possible in the HAZ, because the limited available precipitation and temperature fluctuations (during the day and at night) also occur in alpine mountain systems, so this requires deeper consideration and perhaps new empirical experiments to test ecohydrological relationships in the HAZ.

Readers should note that we performed our field surveys during the spring months of April/May when some species had not leafed out. Therefore, there will be some biases in our PCQM results—notably, two species are missing from our survey data that might be expected to be present. *Potentilla fruticosa* var. *arbuscula* is a common alpine shrub on moister north-facing slopes that had been observed previously in the Khumbu area up to 5,000 m elevation (Byers 2022). Similarly, *Ephedra gerardiana* is a common subshrub on drier slopes in the alpine zone (Byers 2022) and was also missing from our plant survey records.

To what extent are dwarf plant communities in the HAZ spectrally separable based on spectral information from in situ and satellite datasets?

Spectral similarities among dwarf plant species from the same genus (i.e., *J. ecurve* and *J. indica*, *R. anthopogon*, *R. setosum*, and *R. lepidotum*) were observed in the measurements of ALTA and MMR (Figure 7). From in situ measurements, three vegetated LC classes—*Juniperus* spp., *Rhododendron* spp., and meadow—showed visually separable spectral reflectance in red, green, and NIR bands (Figure 7). The spectral separability between *Juniperus* spp. and *Rhododendron* spp. could be explained by the difference between their leaf color and shape: *Juniperus* spp. have dense needle-like leaves, greener than the broad leaves of *Rhododendron* spp. (Mishra et al. 2014). Corresponding with the in situ measurements, the top-of-atmosphere (TOA) reflectance (derived from WV-2) of *Juniperus* spp., *Rhododendron* spp., and meadow was also spectrally separable (Figure 7; $J = 1.99$), particularly in red and NIR bands. Red and NIR bands have been associated strongly with vegetation detection (Carlson and Ripley 1997; Pettorelli et al. 2011) and also have been reported to be useful for alpine vegetation monitoring; for example, the flowering time of wildflowers in the Cascade Range (John et al. 2020),

fractional VC of tundra in the Arctic (Riihimäki, Luoto, and Heiskanen 2019), and alpine meadow phenology in the Alps (Rossi et al. 2019).

However, the challenges of conducting in situ surveys in the Himalayas limited the number of measurements that could be captured during fieldwork. The spectral measurements of plant canopies in this study were only obtained in four bands (blue, green, red, and NIR). The spectral characteristics of plant canopies can reflect their traits and structures (Homolová et al. 2013), which are important metrics for exploring the ecohydrological processes in HAZ, because the temperature and moisture conditions in the microenvironment under dwarf plant canopies predominantly drive their interactions with snow (Löffler et al. 2022).

Also, red-edge and shortwave infrared (SWIR) bands from Sentinel-2 have been identified as being sensitive to plant traits (Ramoelo et al. 2015; Sibanda, Mutanga, and Rouget 2016), such as the concentration of chlorophyll (Sims and Gamon 2002), water, nitrogen, and carbon (Laurin et al. 2016). By band fusion with satellite missions carrying sensors with wider wavelength (e.g., Sentinel-2 or Landsat 8), WV-2 may provide more vegetation characteristics with finer spatial resolution and larger area in HAZ.

Do WV-2 data provide the capacity for land cover classification at the plant community level?

According to the in situ plants species and spectral survey results, mapping vegetation distribution in the HAZ using remote sensing methods requires a satellite data set with a spatial resolution finer than 20 m. The advanced properties of WV-2 (eight multispectral bands and a panchromatic sensor, spatial resolution of 2 m [multispectral] or 0.5 m [panchromatic]) provides potential for mapping vegetation distribution in the HAZ at the plant community level, as demonstrated in this study. Combined with elevation and aspect bands, an LC map of the SNP with high accuracy (OA = 92.56 percent, $\kappa = 0.9$) is shown in Figure 12.

However, some misclassification was observed in the SNP LC map (Figure 12). Firstly, although previous studies demonstrated that the imbalanced LC classes can be used to improve the RF classifier without significantly compromising overall and other per class classification results (Mellor et al. 2015; Noi and Kappas 2017), the rare LC still might be underrepresented relative to more abundant classes, resulting in poor accuracy for minority classes (Chen, Stow, and Gong 2004), which could explain the misclassification between bare soil and meadow in this study (Figure 10). Secondly, the WV-2 image in this study was acquired during the post-monsoon season (November). *Juniperus* spp. and

Rhododendron spp. may have different phenological phases in the pre-monsoon season (March–May) that influence their spectral response and, subsequently, species classification (Shoko and Mutanga 2017). Additional phenology information may reduce some confusion in the LC classification; for example, meadow and bare soil. In this regard, the accuracy of mapping and monitoring the dwarf plant distribution in the HAZ may be improved by identifying the optimal period for monitoring. Constant observations of vegetation traits at some key sites in this zone (e.g., by operating phenocams) could provide useful phenological information to improve the LC classification. Furthermore, the alpine zone in Nepal usually has a growing season that coincides with the Asian monsoon period (Rai et al. 2021), where cloud cover is very high, and therefore this may preclude optical remote sensing from satellite approaches. Radar data from satellite platforms (e.g., Sentinel-1 SAR) with the capacity to penetrate clouds promise to be useful for the development of mapping LC and monitoring snow dynamics in the HAZ, if terrain effects can be reduced and spatial resolution can be improved (Ranson et al. 2001).

How does the plant community composition in the HAZ vary with elevation, aspect, and slope?

We found that dwarf *Rhododendron* spp. preferred to grow on the north-facing slopes, dwarf *Juniperus* spp. were found preferentially on the south-facing slopes, and the reduction in density of *Rhododendron* spp. with altitude increase is slower than *Juniperus* spp. Aspect-related differences in vegetation composition are not uncommon in alpine regions (Dearborn and Danby 2017; Yang, El-Kassaby, and Guan 2020), but variation in exposure to solar radiation may influence environmental variables differently depending on the geographic location of the study (Dearborn and Danby 2017). Yang, El-Kassaby, and Guan (2020) found that in dry mountainous valleys, north-facing slopes were associated with higher soil moisture and nutrient than south-facing slopes, which benefited plant growing and enriched the species diversity in north-facing slopes. In contrast, in subarctic alpine mountains, Dearborn and Danby (2017) found that the plant community composition difference on south- and north-facing slopes was driven primarily by soil temperature, associated with the variation in exposure to solar radiation. Furthermore, the gradient variation of meadow demonstrated in Figure 13 concurs with findings from other shrub encroachment studies in the Himalayas—shrubs encroachment in the alpine Himalayas and meadows at the lower elevations of the alpine zone (between 4,000

and 4,200 m) were encroached most rapidly (Brandt et al. 2013; Zhang et al. 2022). This could explain the peak value of meadow density found around 4,900 m elevation in this study.

It is notable that human activities result in land use change with potentially dramatic effects on vegetation distribution in the HAZ (Xie et al. 2021). Grazing patterns are changing as outmigration limits the available workforce for herding, and the increasing price of cattle is resulting in sell-off of yaks and yak–cow crossbreeds (Byers and Shrestha 2022). Less livestock also means less burning (to increase grass/sedge cover and reduce shrub cover for grazing). The need for yak dung to power stoves for tourist lodges results in livestock being kept closer to lodges and out of the highest pastures (Aryal, Maraseni, and Cockfield 2014). Local protection of dwarf juniper in Khumbu and provision of porter shelters has reduced fuelwood harvesting pressure on dwarf shrub communities (Byers and Shrestha 2022). These activities are predicted to enhance the vegetation changes under a warming climate; for example, expanding greenness at higher elevations and, potentially, shrub encroachment. Hence, exploring the hydrological mechanism and potential impacts between the dwarf plants and snow in the HAZ is particularly vital for the downstream basin safety and resilience. Consideration of land use histories and their effects on vegetation community patterns is beyond the scope of this study but would be a particularly interesting area for further exploration in heavily impacted or managed areas within the HAZ.

Conclusion

In this study in situ spectral measurements, field ecological observations and WV-2 data were analyzed to establish the spectral separabilities within the main dwarf plant communities in the HAZ. According to the spectral information and in situ survey, WV-2 and GLO-30 data sets were combined to assess their capacity for LC classification at the plant community level. To the best of our knowledge, this LC map has the finest spatial resolution (2 m) in the SNP and is the first to characterize the vegetation distribution pattern at the plant community level in the HAZ. Based on the LC map with the optimal band set in the SNP, we analyzed the distribution pattern of three vegetation communities: *Juniperus* spp., *Rhododendron* spp., and meadow. Altitude and aspect are predominantly driving the plant distribution pattern in the HAZ: *Juniperus* spp. are predominantly growing on south- and east-facing slopes, and *Rhododendron* spp. are predominantly growing on north- and west-facing slopes; *Rhododendron* spp. have a wider growing gradient than *Juniperus* spp. in our study area.

Moving forward, to explore the feedback from the Himalayas to climate change, more targeted in situ measurements of metrics identifying ecohydrological interactions between dwarf plants and snow is needed. Citizen science efforts could provide opportunities for wide and effective monitoring in this region. With the support from multisource remote sensing data sets, tracking backwards and forward for decades would be beneficial for further understanding about feedback in response to climate change from this sensitive mountain system.

Acknowledgments

We are grateful to the following institutions and people who contributed for this work: the European Space Agency (ESA), which provided free access to the satellite data in this work (WorldView-2 and Copernicus Digital Elevation Model), and Dr Dhananjay Regmi and Ram Raj Rijal from The Himalayan Research Expeditions company (Kathmandu, Nepal), who provided reliable local support in Nepal, for which we are grateful. Mahesh Magar and Harkrei Sherpa shared their knowledge about Himalayan mountains and provided excellent local guidance within the Goyko area, which enabled us to gain insights via in situ investigation. Dr. Magdalena Mleczko is thanked for her knowledge about satellite data processing in Google Earth Engine and SNAP.

Disclosure statement

No potential conflict of interest was reported by the authors.

Funding

This work was funded by a co-scholarship within the Chinese Scholarship Council (CSC) and University of Exeter, “The Eco-hydrological Interactions between Vegetation and Snow in the Alpine Himalayan”; funding from a Remote Sensing and Photogrammetry Society (RSPSoc) Bill Barlow Award in 2022; and the University of Exeter Centre for Geography and Environmental Science strategic research funding supported our field trip in Nepal.

ORCID

Ruolin Leng  <http://orcid.org/0000-0002-6394-184X>
Stephan Harrison  <http://orcid.org/0000-0003-2820-7313>
Elizabeth A. Byers  <http://orcid.org/0000-0002-0424-0795>
Karen Anderson  <http://orcid.org/0000-0002-3289-2598>

Author contributions

KA, RL, and SH conceived the idea for this work, following fieldwork with MM and HR in the Khumbu region of Nepal. RL, EB, KA, and MM provided knowledge about ecological identification of alpine plants. RL analyzed and visualized the in situ data and satellite data set. RL and KA collaboratively drafted the initial manuscript. KA, SH, and EB provided

feedback on manuscript drafts. RR provided local support for the field logistics in Nepal, obtained permits, and acted as a national park liaison for conducting the in situ survey.

References

- Adam, E., O. Mutanga, J. Odindi, and E. M. Abdel-Rahman. 2014. Land-use/cover classification in a heterogeneous coastal landscape using RapidEye imagery: Evaluating the performance of random forest and support vector machines classifiers. *International Journal of Remote Sensing* 35, no. 10: 3440–58. doi:10.1080/01431161.2014.903435.
- Adler, C., P. Wester, I. Bhatt, C. Huggel, G. E. Insarov, M. D. Morecroft, V. Muccione, and A. Prakash. 2022. Cross-Chapter Paper 5: Mountains. In *Climate Change 2022: Impacts, Adaptation and Vulnerability. Contribution of Working Group II to the Sixth Assessment Report of the Intergovernmental Panel on Climate Change*, ed. D.C. Roberts, M. Tignor, E.S. Poloczanska, K. Mintenbeck, A. Alegria, M. Craig, S. Langsdorf, S. Löschke, V. Möller, A. Okem, B. Rama, 2273–318. New York: Cambridge University Press. doi:10.1017/9781009325844.022.
- Anderson, K., D. Fawcett, A. Cugulliere, S. Benford, D. Jones, and R. Leng. 2020. Vegetation expansion in the subnival Hindu Kush Himalaya. *Global Change Biology* 26, no. 3: 1608–25. doi:10.1111/gcb.14919.
- Anderson, K., and N. J. Kuhn. 2008. Variations in soil structure and reflectance during a controlled crusting experiment. *International Journal of Remote Sensing* 29, no. 12: 3457–75. doi:10.1080/01431160701767435.
- An, X., H. Lu, and G. Chu. 2015. Surface soil phytoliths as vegetation and altitude indicators: A study from the southern Himalaya. *Scientific Reports* 5, no. 1: 1–13. doi:10.1038/srep15523
- Araya-López, R. A., J. Lopatin, F. E. Fassnacht, and H. J. Hernández. 2018. Monitoring Andean high altitude wetlands in central Chile with seasonal optical data: A comparison between Worldview-2 and Sentinel-2 imagery. *ISPRS Journal of Photogrammetry and Remote Sensing* 145: 213–24. doi:10.1016/j.isprsjprs.2018.04.001.
- Aryal, S., G. Cockfield, and T. N. Maraseni. 2016. Perceived changes in climatic variables and impacts on the transhumance system in the Himalayas. *Climate and Development* 8, no. 5: 435–46. doi:10.1080/17565529.2015.1040718.
- Aryal, S., T. N. Maraseni, and G. Cockfield. 2014. Sustainability of transhumance grazing systems under socio-economic threats in Langtang, Nepal. *Journal of Mountain Science* 11: 1023–34. doi:10.1007/s11629-013-2684-7.
- Batar, A. K., T. Watanabe, and A. Kumar. 2017. Assessment of land-use/land-cover change and forest fragmentation in the Garhwal Himalayan Region of India. *Environments* 4, no. 2: 34. doi:10.3390/environments4020034.
- Bolch, T., A. Kulkarni, A. Käab, C. Huggel, F. Paul, J. G. Cogley, H. Frey, J. S. Kargel, K. Fujita, and M. Scheel. 2012. The state and fate of Himalayan glaciers. *Science* 336, no. 6079: 310–4. doi:10.1126/science.1215828.
- Brandt, J. S., M. A. Haynes, T. Kuemmerle, D. M. Waller, and V. C. Radeloff. 2013. Regime shift on the roof of the world: Alpine meadows converting to shrublands in the southern Himalayas. *Biological Conservation* 158: 116–27. doi:10.1016/j.biocon.2012.07.026.
- Byers, E. A. 2022. *Wildflowers of Mount Everest: A field guide to the trees, shrubs, and wildflowers of Sagarmatha National Park (mobile app)*. Nepal: High Country Apps, LLC, in partnership with the Flora of Nepal Project and the Department of National Parks and Wildlife Conservation.
- Byers, A. C., and M. Shrestha. 2022. Conservation and restoration of Alpine ecosystems in the Himalaya. In *Tourism and development in the Himalaya: Social, environmental, and economic forces*, ed. G. P. Nyaupane and D. J. Timothy, 55–73, 328. Oxon and New York: Routledge.
- Carlson, T. N., and D. A. Ripley. 1997. On the relation between NDVI, fractional vegetation cover, and leaf area index. *Remote Sensing of Environment* 62, no. 3: 241–52. doi:10.1016/S0034-4257(97)00104-1.
- Casella, E., J. Drechsel, C. Winter, M. Benninghoff, and A. Rovere. 2020. Accuracy of sand beach topography surveying by drones and photogrammetry. *Geo-Marine Letters* 40: 255–68. doi:10.1007/s00367-020-00638-8.
- Chen, D., D. A. Stow, and P. Gong. 2004. Examining the effect of spatial resolution and texture window size on classification accuracy: An urban environment case. *International Journal of Remote Sensing* 25, no. 11: 2177–92. doi:10.1080/01431160310001618464.
- Cottam, G., and J. T. Curtis. 1956. The use of distance measures in phytosociological sampling. *Ecology* 37, no. 3: 451–60. doi:10.2307/1930167.
- Cuellar, A. C., L. Cenci, C. Santella, and C. Albinet. 2022. Evaluating the Copernicus Dem dataset potential for the identification of (flash) flood-prone areas by using a geomorphological approach. IGARSS 2022-2022 IEEE International Geoscience and Remote Sensing Symposium, July 17-22, in Kuala Lumpur, Malaysia.
- Cunliffe, A. M., R. E. Brazier, and K. Anderson. 2016. Ultra-fine grain landscape-scale quantification of dryland vegetation structure with drone-acquired structure-from-motion photogrammetry. *Remote Sensing of Environment* 183: 129–43. doi:10.1016/j.rse.2016.05.019.
- Dearborn, K. D., and R. K. Danby. 2017. Aspect and slope influence plant community composition more than elevation across forest-tundra ecotones in subarctic Canada. *Journal of Vegetation Science* 28, no. 3: 595–604. doi:10.1111/jvs.12521.
- Deutsch, C. V., and A. G. Journel. 1992. *GSLIB: Geostatistical Software Library and User's Guide*. New York: Oxford University Press.
- Deval, K., and P. K. Joshi. 2022. Vegetation type and land cover mapping in a semi-arid heterogeneous forested wetland of India: Comparing image classification algorithms. *Environment, Development and Sustainability* 24, no. 3: 3947–66. doi:10.1007/s10668-021-01596-6.
- Dolezal, J., M. Dvorsky, M. Kopecky, P. Liancourt, I. Hiiesalu, M. Macek, J. Altman, Z. Chlumská, K. Rehakova, and K. Capkova. 2016. Vegetation dynamics at the upper elevational limit of vascular plants in Himalaya. *Scientific Reports* 6, no. 1: 1–13. doi:10.1038/srep24881.
- Duffy, J. P., J. D. Shutler, M. J. Witt, L. DeBell, and K. Anderson. 2018. Tracking fine-scale structural changes in coastal dune morphology using kite aerial photography and uncertainty-assessed structure-from-motion photogrammetry. *Remote Sensing* 10, no. 9: 1494. doi:10.3390/rs10091494.
- Emanuel, R. E., A. G. Hazen, B. L. McGlynn, and K. G. Jencso. 2014. Vegetation and topographic influences on the connectivity of shallow groundwater between hillslopes and streams. *Ecohydrology* 7, no. 2: 887–95. doi:10.1002/eco.1409.

- Erinjery, J. J., M. Singh, and R. Kent. 2018. Mapping and assessment of vegetation types in the tropical rain forests of the Western Ghats using multispectral Sentinel-2 and SAR Sentinel-1 satellite imagery. *Remote Sensing of Environment* 216: 345–54. doi:10.1016/j.rse.2018.07.006
- Fatichi, S., C. Pappas, and V. Y. Ivanov. 2016. Modeling plant–water interactions: An ecohydrological overview from the cell to the global scale. *Wiley Interdisciplinary Reviews* 3: 327–68. doi:10.1002/wat2.1125.
- Francini, S., R. E. McRoberts, F. Giannetti, M. Mencucci, M. Marchetti, G. Scarascia Mugnozza, and G. Chirici. 2020. Near-real time forest change detection using PlanetScope imagery. *European Journal of Remote Sensing* 53, no. 1: 233–44. doi:10.1080/22797254.2020.1806734.
- Ghimire, B., K. P. Mainali, H. D. Lekhak, R. P. Chaudhary, and A. K. Ghimeray. 2010. Regeneration of *Pinus wallichiana* AB Jackson in a trans-Himalayan dry valley of north-central Nepal. *Himalayan Journal of Sciences* 6, no. 8: 19–26. doi:10.3126/hjs.v6i8.1798.
- Graae, B. J., K. O. Nystuen, V. Vandvik, and A. E. Eycott. 2022. Effects of climate change on regeneration of plants from seeds in boreal, subarctic, and subalpine regions. In *Plant regeneration from seeds*, 19–32. Dordrecht: Elsevier.
- Guth, P. L., and T. M. Geoffroy. 2021. LiDAR point cloud and ICESat-2 evaluation of 1 second global digital elevation models: Copernicus wins. *Transactions in GIS* 25, no. 5: 2245–61. doi:10.1111/tgis.12825.
- Hamid, M., A. A. Khuroo, A. H. Malik, R. Ahmad, C. P. Singh, J. Dolezal, and S. M. Haq. 2020. Early evidence of shifts in alpine summit vegetation: A case study from Kashmir Himalaya. *Frontiers in Plant Science* 11: 421. doi:10.3389/fpls.2020.00421.
- Homolová, L., Z. Malenovský, J. G. Clevers, G. García-Santos, and M. E. Schaepman. 2013. Review of optical-based remote sensing for plant trait mapping. *Ecological Complexity* 15: 1–16. doi:10.1016/j.ecocom.2013.06.003.
- Immerzeel, W., L. Petersen, S. Ragetti, and F. Pellicciotti. 2014. The importance of observed gradients of air temperature and precipitation for modeling runoff from a glacierized watershed in the Nepalese Himalayas. *Water Resources Research* 50: 2212–26. doi:10.1002/2013WR014506.
- Ives, J. D., and B. Messerli. 1990. Progress in theoretical and applied mountain research, 1973–1989, and major future needs. *Mountain Research and Development* 10, no. 2: 101–27.
- Jafari, S. M., S. Zarre, and S. K. Alavipanah. 2013. Woody species diversity and forest structure from lowland to montane forest in Hyrcanian forest ecoregion. *Journal of Mountain Science* 10: 609–20. doi:10.1007/s11629-013-2652-2.
- Jawak, S. D., A. J. Luis, P. T. Fretwell, P. Convey, and U. A. Durairajan. 2019. Semiautomated detection and mapping of vegetation distribution in the Antarctic environment using spatial-spectral characteristics of WorldView-2 imagery. *Remote Sensing* 11, no. 16: 1909. doi:10.3390/rs11161909.
- Ji, X., and X. Niu. 2014. The attribute accuracy assessment of land cover data in the National Geographic Conditions Survey. *ISPRS Annals of the Photogrammetry, Remote Sensing and Spatial Information Sciences* 2, no. 4: 35. doi:10.5194/isprsannals-II-4-35-2014.
- John, A., J. Ong, E. J. Theobald, J. D. Olden, A. Tan, and J. HilleRisLambers. 2020. Detecting montane flowering phenology with CubeSat imagery. *Remote Sensing* 12, no. 18: 2894. doi:10.3390/rs12182894.
- Julitta, T., E. Cremonese, M. Migliavacca, R. Colombo, M. Galvagno, C. Siniscalco, M. Rossini, F. Fava, S. Cogliati, and U. M. Di Cella. 2014. Using digital camera images to analyse snowmelt and phenology of a subalpine grassland. *Agricultural and Forest Meteorology* 198: 116–25. doi:10.1016/j.agrformet.2014.08.007.
- Karasiak, N. 2017. *dzetsaka*: Classification tool. Git-hub. <https://github.com/nkarasiak/dzetsaka>
- Kavzoglu, T., M. Y. Erdemir, and H. Tonbul. 2017. Classification of semiurban landscapes from very high-resolution satellite images using a regionalized multiscale segmentation approach. *Journal of Applied Remote Sensing* 11, no. 3: 035016. doi:10.1117/1.JRS.11.035016.
- Keim, R., A. Skaugset, and M. Weiler. 2006. Storage of water on vegetation under simulated rainfall of varying intensity. *Advances in Water Resources* 29, no. 7: 974–86. doi:10.1016/j.advwatres.2005.07.017.
- Koh, L. P., and S. A. Wich. 2012. Dawn of drone ecology: Low-cost autonomous aerial vehicles for conservation. *Tropical Conservation Science* 5, no. 2: 121–32. doi:10.1177/194008291200500202.
- Körner, C. 2021. *Alpine plant life: Functional plant ecology of high mountain ecosystems*. Berlin: Springer Nature.
- Kumar, V., T. Shukla, M. Mehta, D. Dobhal, M. P. S. Bisht, and S. Nautiyal. 2021. Glacier changes and associated climate drivers for the last three decades, Nanda Devi region, Central Himalaya, India. *Quaternary International* 575: 213–26. doi:10.1016/j.quaint.2020.06.017.
- Kutiél, P., and H. Lavee. 1999. Effect of slope aspect on soil and vegetation properties along an aridity transect. *Israel Journal of Plant Sciences* 47, no. 3: 169–78.
- Laurin, G. V., N. Puletti, W. Hawthorne, V. Liesenberg, P. Corona, D. Papale, Q. Chen, and R. Valentini. 2016. Discrimination of tropical forest types, dominant species, and mapping of functional guilds by hyperspectral and simulated multispectral Sentinel-2 data. *Remote Sensing of Environment* 176: 163–76. doi:10.1016/j.rse.2016.01.017.
- Leng, R., S. Harrison, and K. Anderson. 2022. Himalayan alpine ecohydrology: An urgent scientific concern in a changing climate. *Ambio* 52: 390–410. doi:10.1007/s13280-022-01792-2.
- Löffler, J., E. C. Albrecht, S. Dobbert, R. Pape, and D. Wundram. 2022. Dendrometer measurements of Mediterranean-alpine dwarf shrubs and microenvironmental drivers of plant growth—Dataset from long-term alpine ecosystem research in the Sierra Nevada, Spain (LTAER-ES). *Erdkunde* 76: DP311202. doi:10.3112/erdkunde.2022.dp.01.
- Madonsela, S., M. A. Cho, R. Mathieu, O. Mutanga, A. Ramoelo, Z. Kaszta, R. Van De Kerchove, and E. Wolff. 2017. Multi-phenology WorldView-2 imagery improves remote sensing of Savannah tree species. *International Journal of Applied Earth Observation and Geoinformation* 58: 65–73. doi:10.1016/j.jag.2017.01.018.
- Mären, I. E., S. Karki, C. Prajapati, R. K. Yadav, and B. B. Shrestha. 2015. Facing north or south: Does slope aspect impact forest stand characteristics and soil properties in a semiarid trans-Himalayan valley? *Journal of Arid Environments* 121: 112–23. doi:10.1016/j.jaridenv.2015.06.004.
- McLaren, J. R., K. M. Buckeridge, M. J. van de Weg, G. R. Shaver, J. P. Schimel, and L. Gough. 2017. Shrub encroachment in Arctic tundra: *Betula nana* effects on above- and belowground litter decomposition. *Ecology* 98, no. 5: 1361–76. doi:10.1002/ecy.1790.

- Mellor, A., S. Boukir, A. Haywood, and S. Jones. 2015. Exploring issues of training data imbalance and mislabeling on random forest performance for large area land cover classification using the ensemble margin. *ISPRS Journal of Photogrammetry and Remote Sensing* 105: 155–68. doi:10.1016/j.isprsjprs.2015.03.014.
- Milton, E. J., M. E. Schaepman, K. Anderson, M. Kneubühler, and N. Fox. 2009. Progress in field spectroscopy. *Remote Sensing of Environment* 113: S92–S109. doi:10.1016/j.rse.2007.08.001.
- Mishra, V., D. Kumar, A. R. Ganguly, J. Sanjay, M. Mujumdar, R. Krishnan, and R. D. Shah. 2014. Reliability of regional and global climate models to simulate precipitation extremes over India. *Journal of Geophysical Research: Atmospheres* 119, no. 15: 9301–23. doi:10.1002/2014JD021636.
- Mishra, N. B., and K. P. Mainali. 2017. Greening and browning of the Himalaya: Spatial patterns and the role of climatic change and human drivers. *Science of the Total Environment* 587: 326–39. doi:10.1016/j.scitotenv.2017.02.156.
- Mishra, N. B., K. P. Mainali, B. B. Shrestha, J. Radenz, and D. Karki. 2018. Species-level vegetation mapping in a Himalayan treeline ecotone using unmanned aerial system (UAS) imagery. *ISPRS International Journal of Geo-Information* 7, no. 11: 445. doi:10.3390/ijgi7110445.
- Misra, G., F. Cawkwell, and A. Wingler. 2020. Status of phenological research using Sentinel-2 data: A review. *Remote Sensing* 12, no. 17: 2760. doi:10.3390/rs12172760.
- Mitkari, K. V., M. K. Arora, R. K. Tiwari, S. Sofat, H. S. Gusain, and S. P. Tiwari. 2022. Large-scale debris cover glacier mapping using multisource object-based image analysis approach. *Remote Sensing* 14, no. 13: 3202. doi:10.3390/rs14133202
- Nandy, S., S. Ghosh, S. P. S. Kushwaha, and A. Senthil Kumar. 2019. Remote sensing-based forest biomass assessment in northwest Himalayan landscape. In *Remote Sensing of Northwest Himalayan Ecosystems*, 285–311. Singapore: Springer.
- Nandy, S., R. Srinet, and H. Padalia. 2021. Mapping forest height and aboveground biomass by integrating ICESat-2, Sentinel-1 and Sentinel-2 data using Random Forest algorithm in northwest Himalayan foothills of India. *Geophysical Research Letters* 48, no. 14: e2021GL093799. doi:10.1029/2021GL093799.
- Nayava, J. L. 1980. Rainfall in Nepal. *Himalayan Review* 12: 1–18.
- Nie, Y., H. D. Pritchard, Q. Liu, T. Hennig, W. Wang, X. Wang, S. Liu, S. Nepal, D. Samyn, and K. Hewitt. 2021. Glacial change and hydrological implications in the Himalaya and Karakoram. *Nature Reviews Earth & Environment* 2, no. 2: 91–106. doi:10.1038/s43017-020-00124-w.
- Noi, P., and M. Kappas. 2017. Comparison of random forest, k-nearest neighbor, and support vector machine classifiers for land cover classification using Sentinel-2 imagery. *Sensors* 18, no. 1: 18. doi:10.3390/s18010018.
- Núñez, P. Á., B. Silva, M. Schulz, R. Rollenbeck, and J. Bendix. 2021. Evapotranspiration estimates for two tropical mountain forest using high spatial resolution satellite data. *International Journal of Remote Sensing* 42, no. 8: 2940–62. doi:10.1080/01431161.2020.1864058.
- Oliver, M. A., and R. Webster. 2014. A tutorial guide to geostatistics: Computing and modelling variograms and kriging. *Catena* 113: 56–69. doi:10.1016/j.catena.2013.09.006.
- Pebesma, E. J., and B. Gräler. 2015. Spatio-temporal geostatistics using gstat. Institute for Geoinformatics University of Münster. <http://cran.r-project.org/web/packages/gstat/vignettes/st.pdf>.
- Perry, L. B., T. Matthews, H. Guy, I. Koch, A. Khadka, A. C. Elmore, D. Shrestha, S. Tuladhar, S. K. Baidya, and S. Maharjan. 2020. Precipitation characteristics and moisture source regions on Mt. Everest in the Khumbu, Nepal. *One Earth* 3, no. 5: 594–607. doi:10.1016/j.oneear.2020.10.011.
- Pettorelli, N., S. Ryan, T. Mueller, N. Bunnefeld, B. Jędrzejewska, M. Lima, and K. Kausrud. 2011. The normalized difference vegetation index (NDVI): Unforeseen successes in animal ecology. *Climate Research* 46, no. 1: 15–27. doi:10.3354/cr00936.
- Pu, R., and S. Landry. 2012. A comparative analysis of high spatial resolution IKONOS and WorldView-2 imagery for mapping urban tree species. *Remote Sensing of Environment* 124: 516–33. doi:10.1016/j.rse.2012.06.011.
- QGIS.org. 2022. QGIS geographic information system. QGIS Association. <http://www.qgis.org>.
- Rai, M. R., A. Chidhaisong, C. Ekkawatpanit, and P. Varnakovida. 2021. Assessing climate change trends and their relationships with Alpine vegetation and surface water dynamics in the Everest region, Nepal. *Atmosphere* 12, no. 8: 987. doi:10.3390/atmos12080987.
- Ramoelo, A., M. Cho, R. Mathieu, and A. K. Skidmore. 2015. Potential of Sentinel-2 spectral configuration to assess rangeland quality. *Journal of Applied Remote Sensing* 9, no. 1: 94096. doi:10.1117/1.JRS.9.094096.
- Rana, M. S., S. Samant, and Y. Rawat. 2011. Plant communities and factors responsible for vegetation pattern in an alpine area of the northwestern Himalaya. *Journal of Mountain Science* 8: 817–26. doi:10.1007/s11629-011-2078-7.
- Ranson, K. J., G. Sun, V. I. Kharuk, and K. Kovacs. 2001. Characterization of forests in Western Sayani Mountains, Siberia from SIR-C SAR data. *Remote Sensing of Environment* 75, no. 2: 188–200. doi:10.1016/S0034-4257(00)00166-8.
- Rapinel, S., B. Clément, S. Magnanon, V. Sellin, and L. Hubert-Moy. 2014. Identification and mapping of natural vegetation on a coastal site using a Worldview-2 satellite image. *Journal of Environmental Management* 144: 236–46. doi:10.1016/j.jenvman.2014.05.027.
- Rashid, M., M. A. Lone, and S. A. Romshoo. 2011. Geospatial tools for assessing land degradation in Budgam district, Kashmir Himalaya, India. *Journal of Earth System Science* 120: 423–33. doi:10.1007/s12040-011-0085-2.
- Rasool, R., A. Fayaz, M. Ul Shafiq, H. Singh, and P. Ahmed. 2021. Land use land cover change in Kashmir Himalaya: Linking remote sensing with an indicator based DPSIR approach. *Ecological Indicators* 125: 107447. doi:10.1016/j.ecolind.2021.107447.
- Reese, H., M. Nyström, K. Nordkvist, and H. Olsson. 2014. Combining airborne laser scanning data and optical satellite data for classification of alpine vegetation. *International Journal of Applied Earth Observation and Geoinformation* 27: 81–90. doi:10.1016/j.jag.2013.05.003.
- Richards, J. A. 2013. Feature reduction. In *Remote Sensing Digital Image Analysis: An Introduction*, 343–80. Berlin: Springer.
- Riihimäki, H., M. Luoto, and J. Heiskanen. 2019. Estimating fractional cover of tundra vegetation at multiple scales using unmanned aerial systems and optical satellite data. *Remote Sensing of Environment* 224: 119–32. doi:10.1016/j.rse.2019.01.030.

- Rossi, M., G. Niedrist, S. Asam, G. Tonon, E. Tomelleri, and M. Zebisch. 2019. A comparison of the signal from diverse optical sensors for monitoring alpine grassland dynamics. *Remote Sensing* 11, no. 3: 296. doi:10.3390/rs11030296.
- RStudio Team. 2015. *RStudio, integrated development for R*. Boston, MA: RStudio, Inc. <http://www.rstudio.com/>.
- Saco, P. M., J. F. Rodríguez, M. Moreno-de Las Heras, S. Keesstra, S. Azadi, S. Sandi, J. Baartman, J. Rodrigo-Comino, and M. J. Rossi. 2020. Using hydrological connectivity to detect transitions and degradation thresholds: Applications to dryland systems. *Catena* 186: 104354. doi:10.1016/j.catena.2019.104354.
- Saha, A. K., M. K. Arora, E. Csaplovics, and R. P. Gupta. 2005. Land cover classification using IRS LISS III image and DEM in a rugged terrain: A case study in Himalayas. *Geocarto International* 20, no. 2: 33–40. doi:10.1080/10106040508542343.
- Sanam, H., A. K. Mathai, and G. Lakshmanan. 2023. Multi-resolution remote sensing for the specieslevel classification of mangroves. 2023 International Conference on Machine Intelligence for GeoAnalytics and Remote Sensing (MIGARS), January 1-4, in Hyderabad, India.
- Schmidt, K. S., and A. K. Skidmore. 2003. Spectral discrimination of vegetation types in a coastal wetland. *Remote Sensing of Environment* 85, no. 1: 92–108. doi:10.1016/S0034-4257(02)00196-7.
- Serbin, S. P., A. Singh, B. E. McNeil, C. C. Kingdon, and P. A. Townsend. 2014. Spectroscopic determination of leaf morphological and biochemical traits for northern temperate and boreal tree species. *Ecological Applications* 24, no. 7: 1651–69. doi:10.1890/13-2110.1.
- Shahi, K., H. Z. M. Shafri, and A. Hamedianfar. 2017. Road condition assessment by OBIA and feature selection techniques using very high-resolution WorldView-2 imagery. *Geocarto International* 32, no. 12: 1389–406. doi:10.1080/10106049.2016.1213888.
- Shoko, C., and O. Mutanga. 2017. Examining the strength of the newly-launched Sentinel 2 MSI sensor in detecting and discriminating subtle differences between C3 and C4 grass species. *ISPRS Journal of Photogrammetry and Remote Sensing* 129: 32–40. doi:10.1016/j.isprsjprs.2017.04.016.
- Shrestha, U. B., S. Gautam, and K. S. Bawa. 2012. Widespread climate change in the Himalayas and associated changes in local ecosystems. *PloS one* 7, no. 5: e36741. doi:10.1371/journal.pone.0036741.
- Sibanda, M., O. Mutanga, and M. Rouget. 2016. Discriminating rangeland management practices using simulated HypSIRI, Landsat 8 OLI, Sentinel 2 MSI, and Venus spectral data. *IEEE Journal of Selected Topics in Applied Earth Observations and Remote Sensing* 9, no. 9: 3957–69. doi:10.1109/JSTARS.2016.2574360.
- Sims, D. A., and J. A. Gamon. 2002. Relationships between leaf pigment content and spectral reflectance across a wide range of species, leaf structures and developmental stages. *Remote Sensing of Environment* 81, no. 2–3: 337–54. doi:10.1016/S0034-4257(02)00010-X.
- Singh, H., and A. C. Pandey. 2021. Land deformation monitoring using optical remote sensing and PS-InSAR technique nearby Gangotri glacier in higher Himalayas. *Modeling Earth Systems and Environment* 7: 221–33. doi:10.1007/s40808-020-00889-5.
- Smith, W. K., M. P. Dannenberg, D. Yan, S. Herrmann, M. L. Barnes, G. A. Barron-Gafford, J. A. Biederman, S. Ferrenberg, A. M. Fox, and A. Hudson. 2019. Remote sensing of dryland ecosystem structure and function: Progress, challenges, and opportunities. *Remote Sensing of Environment* 233: 111401. doi:10.1016/j.rse.2019.111401.
- Suchá, R., L. Jakešová, L. Kupková, and L. Červená. 2016. Classification of vegetation above the tree line in the Krkonoše Mts. National Park using remote sensing multi-spectral data. *Acta Universitatis Carolinae, Geographica* 51: 113–29.
- Telwala, Y., B. W. Brook, K. Manish, and M. K. Pandit. 2013. Climate-induced elevational range shifts and increase in plant species richness in a Himalayan biodiversity epicentre. *PLoS ONE* 8, no. 2: e57103. doi:10.1371/journal.pone.0057103
- Terskaia, A., R. J. Dial, and P. F. Sullivan. 2020. Pathways of tundra encroachment by trees and tall shrubs in the western Brooks Range of Alaska. *Ecography* 43, no. 5: 769–78. doi:10.1111/ecog.05015.
- Thomson, E. R., M. P. Spiegel, I. Althuizen, P. Bass, S. Chen, A. Chmurzynski, H. Halbritter, et al. 2021. Multiscale mapping of plant functional groups and plant traits in the High Arctic using field spectroscopy, UAV imagery and Sentinel-2A data. *Environmental Research Letters* 16, no. 5: 055006. doi:10.1088/1748-9326/abf464.
- Tomaszewska, M. A., L. H. Nguyen, and G. M. Henebry. 2020. Land surface phenology in the highland pastures of montane Central Asia: Interactions with snow cover seasonality and terrain characteristics. *Remote Sensing of Environment* 240: 111675. doi:10.1016/j.rse.2020.111675.
- Treiman, A. H. 2000. *ALTA reflectance spectrometer: Introduction and classroom lessons*. Houston: Lunar and Planetary Institute.
- Uddin, K., H. L. Shrestha, M. Murthy, B. Bajracharya, B. Shrestha, H. Gilani, S. Pradhan, and B. Dangol. 2015. Development of 2010 national land cover database for the Nepal. *Journal of Environmental Management* 148: 82–90. doi:10.1016/j.jenvman.2014.07.047.
- Urdike, T., and C. Comp. 2010. Radiometric use of WorldView-2 imagery. *Technical Note*. Longmont, Colorado: DigitalGlobe.
- Verdonen, M., L. T. Berner, B. C. Forbes, and T. Kumpula. 2020. Periglacial vegetation dynamics in Arctic Russia: Decadal analysis of tundra regeneration on landslides with time series satellite imagery. *Environmental Research Letters* 15, no. 10: 105020. doi:10.1088/1748-9326/abb500.
- Wacker, A. G., and D. A. Landgrebe. 1971. Minimum distance classification in remote sensing. *Laboratory for Application of Remote Sensing* 1, no. 1: 1–25.
- Walker, J. J., K. M. De Beurs, and R. H. Wynne. 2014. Dryland vegetation phenology across an elevation gradient in Arizona, USA, investigated with fused MODIS and Landsat data. *Remote Sensing of Environment* 144: 85–97. doi:10.1016/j.rse.2014.01.007.
- Walker, M. D., C. H. Wahren, R. D. Hollister, G. H. Henry, L. E. Ahlquist, J. M. Alatalo, M. S. Bret-Harte, M. P. Calef, T. V. Callaghan, and A. B. Carroll. 2006. Plant community responses to experimental warming across the tundra biome. *Proceedings of the National Academy of Sciences* 103, no. 5: 1342–6. doi:10.1073/pnas.0503198103.

- Wheeler, J. A., A. J. Cortes, J. Sedlacek, S. Karrenberg, M. van Kleunen, S. Wipf, G. Hoch, O. Bossdorf, and C. Rixen. 2016. The snow and the willows: Earlier spring snowmelt reduces performance in the low-lying alpine shrub *Salix herbacea*. *Journal of Ecology* 104, no. 4: 1041–50. doi:10.1111/1365-2745.12579.
- Wicaksono, P., and P. A. Aryaguna. 2020. Analyses of inter-class spectral separability and classification accuracy of benthic habitat mapping using multispectral image. *Remote Sensing Applications: Society and Environment* 19: 100335. doi:10.1016/j.rsase.2020.100335.
- Xie, F. D., X. Wu, L. S. Liu, Y. L. Zhang, and B. Paudel. 2021. Land use and land cover change within the Koshi River Basin of the central Himalayas since 1990. *Journal of Mountain Science* 18, no. 1: 159–77.
- Yang, J., Y. A. El-Kassaby, and W. Guan. 2020. The effect of slope aspect on vegetation attributes in a mountainous dry valley, Southwest China. *Scientific Reports* 10, no. 1: 1–11. doi:10.1038/s41598-019-56847-4.
- Zhang, Z., Y. F. Liu, Z. Cui, Z. Huang, Y. Liu, P. A. Leite, et al. 2022. Shrub encroachment impaired the structure and functioning of alpine meadow communities on the Qinghai–Tibetan Plateau. *Land Degradation & Development* 33, no. 14: 2454–63. doi:10.1002/ldr.4323.
- Zou, L., F., Tian, T. Liang, L. Eklundh, X. Tong, T. Tagesson, Y. Dou, T. He, S. Liang, and R. Fensholt. 2023. Assessing the upper elevational limits of vegetation growth in global high-mountains. *Remote Sensing of Environment* 286: 113423. doi:10.1016/j.rse.2022.113423